

## Original Article

**Cite this article:** Carosi R, Montomoli C, Iaccarino S, Cottle JM, Massonne H-J, Nania L, and Simonetti M. Constraining the evolution of shear zones in the Himalayan mid crust in Central–Western Nepal: implications for the tectonic evolution of the Himalayan metamorphic core. *Geological Magazine* <https://doi.org/10.1017/S0016756823000365>

Received: 11 January 2023

Revised: 3 June 2023

Accepted: 5 June 2023




**Keywords:**

Shear zone; petrochronology; Himalaya; High Himalayan Discontinuity; U-Th-Pb monazite dating

**Corresponding author:** Chiara Montomoli;

Email: [chiara.montomoli@unipi.it](mailto:chiara.montomoli@unipi.it)

# Constraining the evolution of shear zones in the Himalayan mid crust in Central–Western Nepal: implications for the tectonic evolution of the Himalayan metamorphic core

Rodolfo Carosi<sup>1</sup> , Chiara Montomoli<sup>1,2</sup> , Salvatore Iaccarino<sup>1</sup> , John M. Cottle<sup>3</sup>, Hans-Joachim Massonne<sup>4</sup>, Laura Nania<sup>5,6</sup> and Matteo Simonetti<sup>7</sup>

<sup>1</sup>Dipartimento di Scienze della Terra, Università di Torino, Torino, Italy; <sup>2</sup>Istituto di Geoscienze e Georisorse, CNR, Pisa, Italy; <sup>3</sup>Department of Earth Science, University of California, Santa Barbara, CA, USA; <sup>4</sup>School of Earth Sciences, China University of Geosciences, Wuhan, China; <sup>5</sup>Dipartimento di Scienze della Terra, Università di Firenze, Firenze, Italy; <sup>6</sup>Geological Survey of Canada, Natural Resources Canada, Ottawa, Canada and <sup>7</sup>Servizio Geologico d'Italia, ISPRA, Roma, Italy

**Abstract**

Structural analysis, petrochronology and metamorphic petrology enable identification and bracketing of the timing of a newly mapped high-temperature ductile shear zone (Jagat Shear Zone (JSZ)) in the Himalayan metamorphic core in Central–Western Nepal. *In situ* U-Th-Pb monazite petrochronology constrains the timing of top-to-the-S/SW shearing between 28–27 Ma and 17 Ma. Burial and prograde metamorphisms in footwall rocks were linked to thrust-sense movement along the JSZ, while the hanging wall rocks were retrogressed and exhumed. The identification and age of the JSZ (as part of a regional system of shear zones: the High Himalayan Discontinuity (HHD)) coupled with the localization and timing of activity of the Main Central Thrust (MCT) (i) fills a gap in tracing the HHD along orogenic strike, (ii) supports the identification of the position and timing of the long-debated MCT and (iii) helps to place the boundaries of the Himalayan metamorphic core and its internal architecture. Thus, our study is a significant step towards a precise identification of the burial, assembly and exhumation mechanisms of the Himalayan metamorphic core.

**1. Introduction**

Tracing first-order lithospheric structures in collisional orogens is challenging due to their complex architecture and tectono-metamorphic history. One example is the position of a major structure in the most classical collisional orogen: the Main Central Thrust zone (MCTz), a first-order tectonic boundary running along the Himalayan belt for ~2400 km along strike (Fig. 1). It separates the metamorphic core (Greater Himalayan Sequence (GHS)) in the hanging wall from the Lesser Himalayan Sequence (LHS) in the footwall. Since the MCTz was defined by Heim and Gansser (1939), its position, age and role in the tectonic evolution of the belt are still debated (Searle *et al.* 2008; Martin, 2017a, 2017b; Mukhopadhyay *et al.* 2017; Carosi *et al.* 2018; Montemagni *et al.* 2018, 2020; Chakraborty *et al.* 2019; Iaccarino *et al.* 2020). According to Godin *et al.* (2006) and Catlos *et al.* (2018, 2020), the age of the MCTz spans between 25 and 18–16 Ma down to nearly 3 Ma (Catlos *et al.* 2001). The localization and timing of the MCTz play a major role in the definition of the tectonic models envisaged for the exhumation of the belt. Several models (Parsons *et al.* 2016a, 2016b and references therein) are based on the contemporaneous activity of the MCT and the South Tibetan Detachment System (STDS), which separates the GHS from the upper Tethyan Himalayan Sequence (THS), so that the age and the structural position of the MCT are fundamental issues (Montomoli *et al.* 2013; Montemagni *et al.* 2019, 2020). Montomoli *et al.* (2015) pointed to the occurrence of a regional-scale structure (High Himalayan Discontinuity (HHD)) within the GHS. Carosi *et al.* (2018) demonstrated that the MCT and HHD are often confused in the literature for the time span from 25–26 Ma to 16 Ma (Godin *et al.* 2006). The univocal position and dating of structural and metamorphic discontinuities in the GHS became key points for unravelling the tectonic evolution of the orogenic belt. A strand of the STDS, the Chame detachment in the Marsyangdi valley (Coleman, 1998; Searle & Godin, 2003; Searle, 2010) (Fig. 2a), has been interpreted as a ramp of the HHD (Walters & Kohn, 2017) so that even the kinematics of shear zones of the upper GHS is challenged. Dating deformation events in tectonites is a major challenge (Müller *et al.* 2000; Williams & Jercinovic, 2002, 2012; Carosi *et al.* 2022; Dumond *et al.* 2022) and *in situ* radiometric dating of mineral (re)crystallization within different fabrics helps to unravel the deformation history (Di Vincenzo *et al.* 2004; Villa, 2016). Metamorphic minerals often show

© The Author(s), 2023. Published by Cambridge University Press. This is an Open Access article, distributed under the terms of the Creative Commons Attribution licence (<http://creativecommons.org/licenses/by/4.0/>), which permits unrestricted re-use, distribution and reproduction, provided the original article is properly cited.



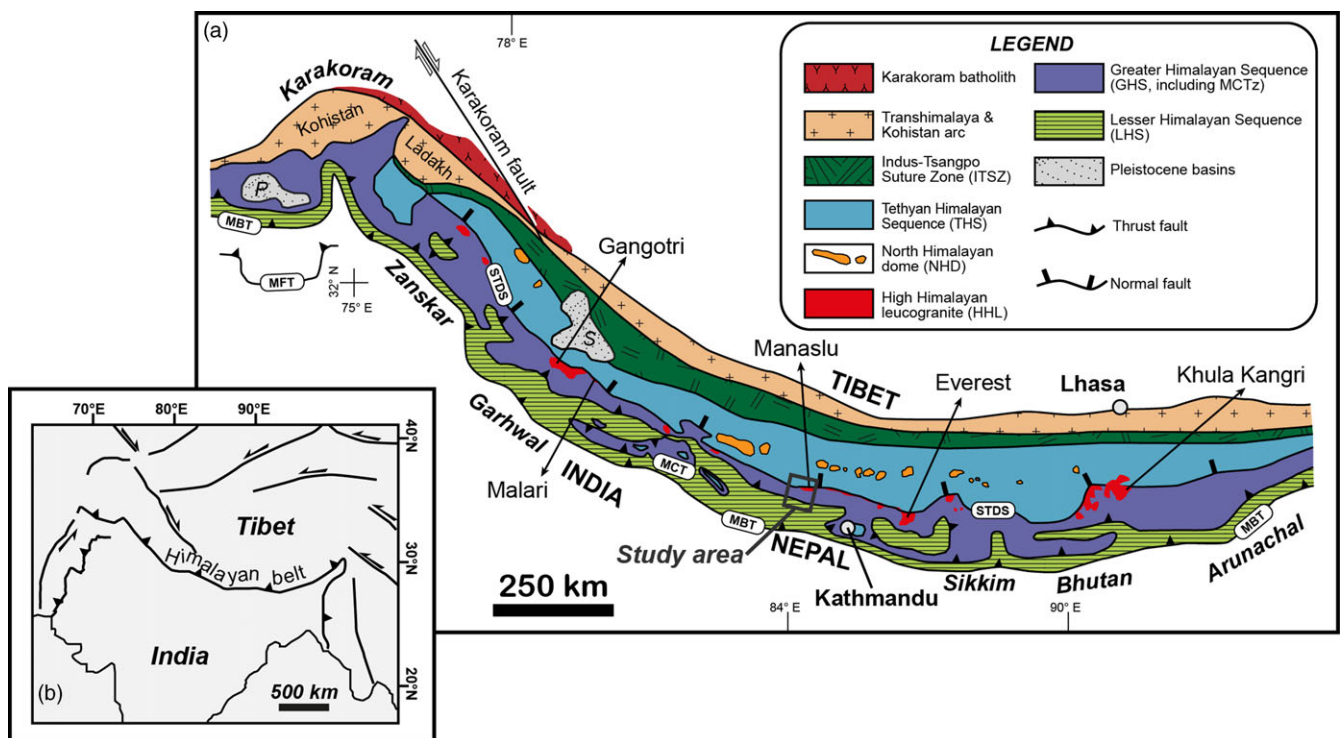


**Figure 1.** (Colour online) (a) Geological map of the Himalaya (modified after Searle, *et al.* 2008; Weinberg, 2016; Searle, 2019) and (b) its geographic position. MFT, Main Frontal Thrust; MBT, Main Boundary Thrust; MCT, Main Central Thrust; STDS, South Tibetan Detachment System; P, Peshawar basin; S, Sutlej basin.

chemical zoning of major and trace elements, and a large spread of dates is obtained, even in a single mineral (Villa *et al.* 2000; Rubatto *et al.* 2001, 2013; Gibson *et al.* 2004; Kohn *et al.* 2005; Pyle *et al.* 2005; Pyle, 2006; Corrie & Kohn, 2011; Kohn, 2016). It is not trivial to link the obtained dates to the different generation of structures. Nevertheless, the complexity in age and mineral chemistry of geochronometers is the key to unravel the history of deformation and metamorphism (Engi, 2017; Schulz, 2021; Dumond *et al.* 2022; Imayama *et al.* 2022). Approaches combining *in situ* U-Th-Pb data, with textural position and geochemical composition of minerals, are useful to date geologic events (e.g., Williams *et al.* 1999, 2007; Gibson *et al.* 2004; Pyle, 2006; Rubatto *et al.* 2013; Kohn *et al.* 2017). In this paper, we focus on laser ablation split stream (LASS) dating (Cottle *et al.* 2012; Kylander-Clark *et al.* 2013) of monazite in metasedimentary rocks affected by high-temperature (amphibolite facies) ductile shear in the metamorphic core of the Himalaya in the Manaslu massif (Central-Western Nepal) (Figs. 1, 2).

The HHD was first recognized in Western Nepal (Carosi *et al.* 2010; Montomoli *et al.* 2013, 2015; see Carosi *et al.* 2018, 2019 for a review), but gaps exist remain in our understanding of its along-strike continuation to the east (Carosi *et al.* 2018; Waters, 2019). In this framework, rocks from the Marsyangdi and Budhi Gandaki valleys in Central Nepal (Fig. 2) were investigated to detect the occurrence and the structural position of a shear zone, which can be correlated with the HHD, and to constrain its age by *in situ* U-Th-Pb dating of monazite.

## 2. Geological setting

### 2.a. The Himalayas

The Himalayas (Fig. 1) developed after the initial collision between the Indian and Eurasian plates at ~59–55 Ma (Le Fort 1975; Green

*et al.* 2008; Hu *et al.* 2016). The orogenic belt is composed of different tectonic units derived from the northern part of the Indian Plate, which were deformed, metamorphosed and accreted at different structural levels south of the Indus-Tsangpo Suture Zone (Hébert *et al.* 2012; Searle, 2019). The zone contains remnants of the Neo-Tethys Ocean that was located between the Indian and Eurasian plates. Five main litho-tectonic units, forming the backbone of the belt, are recognized. To the south, Cenozoic synorogenic sedimentary rocks of the Sub-Himalayan sequence are tectonically overlaid by metasedimentary and meta-igneous rocks of the LHS (Upreti & Le Fort, 1999; Hodges, 2000). A km-thick ductile to ductile-brittle shear zone, the MCTz (Heim & Gansser, 1939; Gansser, 1964; Searle *et al.* 2008; Martin, 2017a, 2017b), separates the mostly greenschist – with minor lower amphibolite-facies rocks of the LHS from the tectonically overlying GHS, which is mainly composed of middle to upper amphibolite facies metasedimentary and meta-igneous rocks (Le Fort, 1975; Hodges, 2000; Carosi *et al.* 2018 and references therein) and represents the metamorphic core of the orogenic belt. Deformation with a top-to-the-S kinematics, linked to the MCTz, affected both the bottom of the GHS and the upper part of the LHS. In the lower part of the GHS garnet- to kyanite-bearing paragneiss and micaschist with subordinate calc-schist, quartzite, impure marble and migmatite occur. The middle portion of the GHS is made of calcisilicate gneiss and marble with minor pelitic and psammitic levels (Fig. 2). The uppermost part of the GHS consists of orthogneiss and aluminosilicate-bearing migmatites. Crustally derived, Oligo-Miocene leucogranite intrusions (Searle, 2010, 2013; Visonà *et al.* 2012; Weinberg, 2016), such as the Manaslu granite (Guillot *et al.* 1995; Cottle *et al.* 2019), are abundant in the upper part of the GHS. Tectonically above the GHS, unmetamorphosed sedimentary rocks (Frank & Fuchs, 1970; Garzanti, 1999) with minor amphibolite facies rocks (Antolín *et al.* 2011; Dunkl

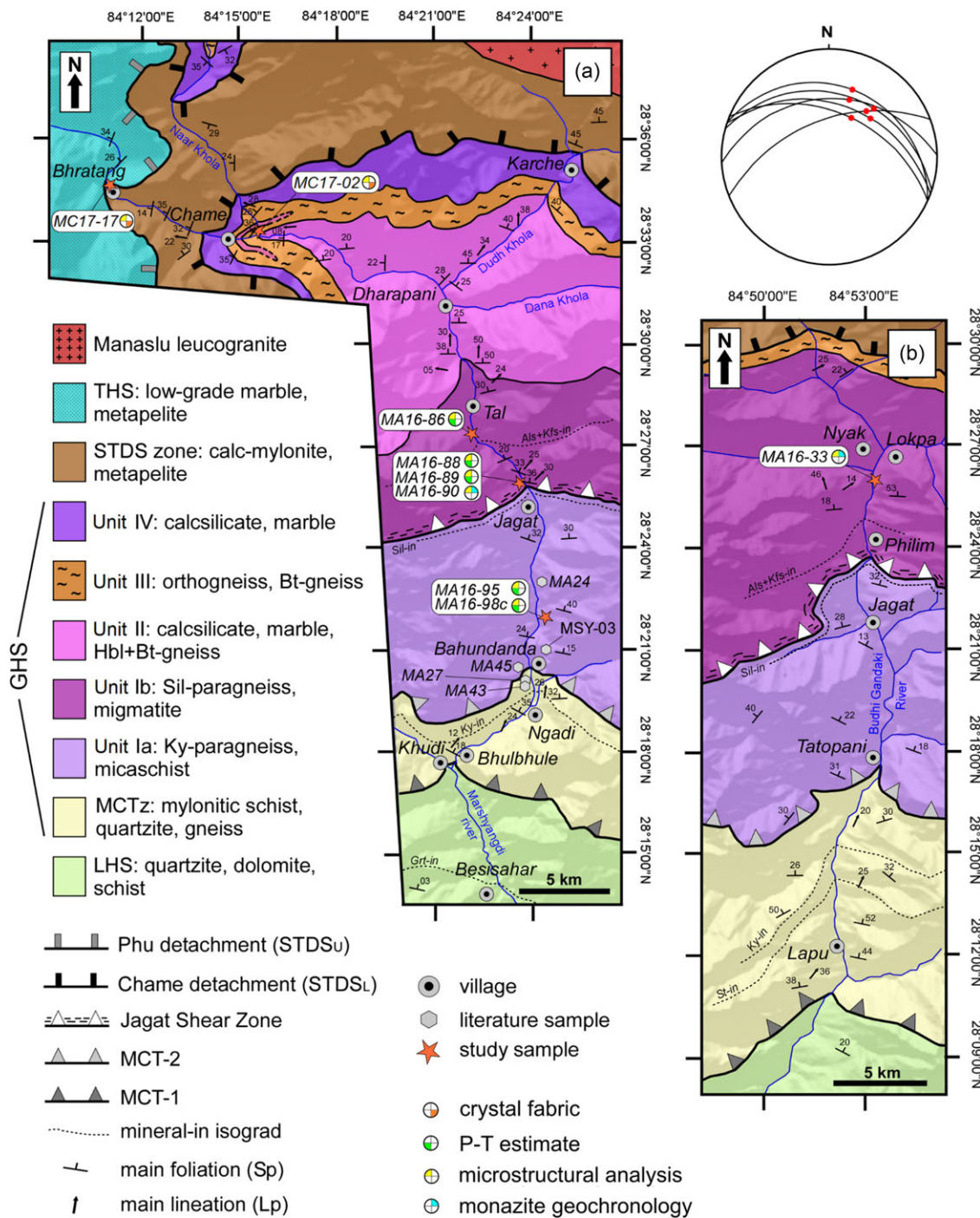


**Figure 2.** (Colour online) (a) Geological map of the Marsyangdi river valley. (b) Geological map of the Budhi Gandaki river valley (after Parsons *et al.* 2016 and our observations) showing the trace of the Jagat Shear Zone (JSZ) and sample locations. On the right-hand side: stereonet (Wulff net, lower hemisphere) of the mylonitic foliation and grain/object lineation (red dots) of the JSZ.

*et al.* 2011; Montomoli *et al.* 2017) of the THS are present. The tectonic boundary between GHS and THS is represented by a system of low-angle ductile shear zones to brittle faults with a normal top-to-the-N or -NE kinematics, referred to the STDS (Burg *et al.* 1984; Burchfiel *et al.* 1992; Carosi *et al.* 1998; Searle *et al.* 2003; Kellett *et al.* 2010, 2019; Searle, 2010; Iaccarino *et al.* 2017b; Nania *et al.* 2022). The occurrence of the STDS at the top of the GHS and of the MCTz at its bottom, as two coeval north-dipping shear zones with opposite kinematics, played a key role in

shaping the Himalayas and exhuming the GHS. These processes are, however, complicated, particularly since ductile contractional shear zones within the GHS were found in several transects across the belt (Carosi *et al.* 2010; Martin *et al.* 2010, 2015; Corrie & Kohn, 2011; Imayama *et al.* 2012, 2022; Montomoli *et al.* 2013, 2015; Ambrose *et al.* 2015; Cottle *et al.* 2015; He *et al.* 2015; Khanal *et al.* 2015; Larson *et al.* 2015; Wang *et al.* 2015, 2016; Zeiger *et al.* 2015; Agustsson *et al.* 2016; Iaccarino *et al.* 2017a; Walters & Kohn, 2017; Goscombe *et al.* 2018; Chakraborty *et al.* 2019; Waters, 2019;

Shrestha *et al.* 2020; Benetti *et al.* 2021) and related to a regional scale tectono-metamorphic discontinuity known as HHD. The HHD occurs in the middle part of the GHS close to the boundary between migmatite and kyanite-bearing paragneiss, with hanging wall rocks showing a higher degree of melting compared to the footwall rocks and with a decoupling in the prograde and retrograde metamorphic history (Montomoli *et al.* 2013, 2015). The activity of the HHD is constrained between 28–27 and 17 Ma and facilitated exhumation of the upper part of the GHS before the initiation of the MCT (Carosi *et al.* 2010; Montomoli *et al.* 2013, 2015).

### 2.b. Localization of the MCT

Mapping, localization, timing and tectono-metamorphic evolution of the MCTz are still debated (Martin, 2017a). Researchers have proposed several criteria for defining the MCTz including lithological, timing of activity, structural and metamorphic criteria. Examples are (i) a 'sharp' litho-tectonic boundary (e.g. Heim & Gansser, 1939) between the medium- to high-grade gneiss (i.e. GHS) and the medium- to low-grade quartzite (LHS); (ii) a metamorphic criterion to identify the MCTz close to the kyanite-in isograd (Le Fort, 1975; Pêcher, 1989); (iii) a protolith boundary, where the MCTz separates rocks with different Nd and Sr isotopic signatures (e.g. Ahmad *et al.* 2000) and with different maximum depositional age based on zircon U-Pb populations (Parrish & Hodges, 1996) and (iv) a structural criteria (Searle *et al.* 2008), where the MCTz is mapped based on strain criteria, that is, the recognition of a strain gradient on distinct deformation localization highlighted by field and microstructural observations (Law *et al.* 2013; Parsons *et al.* 2016a, 2016b, 2016c; Larson *et al.* 2010, 2017; Hunter *et al.* 2019). Frequently, a contractional top-to-the-S high-strain zone corresponds to the base of an inverted metamorphic sequence (Searle *et al.* 2008; Iaccarino *et al.* 2020). Moreover, several authors mapped two different thrusts, MCT-I and MCT-II (Arita, 1983) or Munsiri and Vaikrita thrusts (Valdiya *et al.* 1999) bounding strongly sheared rocks of the MCTz. Probably, a combination of several of them is required to localize the MCTz. The problem of localization of the MCT is particularly evident in our study area as exemplified by the variable locations of the MCT in different studies (Colchen *et al.* 1986; Larson *et al.* 2010, 2011; Martin *et al.* 2015; Parsons *et al.* 2016c).

### 2.c. Study area

The Marsyangdi river and Budhi Gandaki river valleys are located in the Annapurna region of Central-Western Nepal, on the western and the eastern side, of the Manaslu massif and expose the upper part of the LHS, a complete section of the GHS and the lower part of the THS (Colchen *et al.* 1986; Pêcher, 1989, 1991; Coleman, 1996, 1998; Coleman & Hodges, 1998; Parsons *et al.* 2016c). In the Marsyangdi river valley, the LHS, separated from the GHS by the MCTz (Fig. 2), is made of chlorite- to garnet-bearing quartzite. The MCTz is represented by mylonitic schist, quartzite and paragneiss (Pêcher, 1989, 1991; Catlos *et al.* 2001, 2018; Larson *et al.*, 2010; Catlos, 2021; Martin *et al.* 2015; Gibson *et al.* 2016) defining a 2 to 4 km-thick high-strain zone with top-to-the-S kinematics. According to Pêcher (1989) and Catlos (2021), the top of the MCTz is localized just above the kyanite-in isograd. Recent garnet-based pressure-temperature (P-T) paths were presented by Catlos *et al.* (2018), following Catlos *et al.* (2001), for rocks across the MCTz suggesting an increase of both pressure and temperature

traced structurally upwards. Coleman (1998) and Catlos *et al.* (2001) presented monazite U-Pb and Th-Pb ages, respectively, suggesting that the shearing along the MCTz was active between 25–22 Ma and c. 3 Ma. However, the interpretation of the U-Th-Pb dates, obtained by these authors, is dubious due to lack of detailed characterization of the monazite chemical composition (Kohn, 2016). Recent monazite dating by Gibson *et al.* (2016) (their sample MSY-03) yielded ages between 32 and 26 Ma for prograde conditions and between 18–17 Ma and ~ 13 Ma for the exhumation of MCTz rocks.

The GHS in the Marsyangdi river valley (Fig. 2a) is classically subdivided into several formations (Le Fort, 1975; Colchen *et al.* 1986; Pêcher & Le Fort, 1986), now more properly referred as units (Searle & Godin, 2003). The lowest Unit I consists of garnet- to kyanite-bearing paragneiss and micaschist (Unit Ia; 2a) and sillimanite-bearing paragneiss and migmatite (Unit Ib; Fig. 2). Close to the village of Jagat, within Unit I, a ductile shear zone, recognized for the first time in this contribution and described in detail below, splits (Fig. 2a) Unit I (as defined by Corrie & Kohn, 2011) into Unit Ia and Unit Ib. Layered calcsilicate, marble and amphibole-biotite-bearing gneiss (Fig. 2a) constitute Unit II. Unit III is represented by orthogneiss, migmatite and biotite-gneiss (Fig. 2a). According to Coleman (1996), a thin interlayered portion of Unit II splits Unit III into structurally upper and lower parts. Unit IV at the top of the GHS is defined by diopside-amphibole calcsilicate and marble (Fig. 2a). In the studied area, the THS is tectonically separated from the GHS by the STDS which is represented by mylonitic calcsilicate and metapelite sandwiched between a lower shear zone, referred as the Chame detachment as it crops out close to the village of Chame (Coleman, 1996; Parsons *et al.* 2016a, 2016b, 2016c; Fig. 2a), and the upper Phu detachment (Fig. 2a) (Searle & Godin, 2003; Searle, 2010). Low-grade marble and metapelite (Schneider & Marsh, 1993) represent the main lithologies of the THS (Fig. 2a). In the upper part of the Marsyangdi valley, leucogranite dykes and sills, likely linked to the activity of the Manaslu pluton (22–19 Ma, Guillot *et al.* 1994; Cottle *et al.* 2019), are common. A debate exists about the nature, kinematics and tectonic meaning of the Chame detachment, which has been previously interpreted as a ductile branch of the STDS (Coleman, 1996; Coleman & Hodges, 1998; Searle, 2010; Parsons *et al.* 2016a, 2016b, 2016c). In contrast, Walters and Kohn (2017) proposed a reverse-sense (top-to-the-S) kinematic framework for this structure, mainly based on petrological and titanite petrochronological data and interpreted it as an intra-GHS thrust, active in the time span of 25–17 Ma. Thus, it is crucial for bracketing the geological evolution in the area to unambiguously determine the kinematic nature of the Chame detachment.

A similar setting is recognizable in the Budhi Gandaki river valley (Larson *et al.* 2010, 2011) on the eastern side of the Manaslu massif (Fig. 2b). The main differences to the Marsyangdi valley are the virtual absence of calcsilicate and marble of Unit II (Colchen *et al.* 1986) and the occurrence of carbonate-bearing lithologies within the MCTz (Colchen *et al.* 1986; Nania, 2021). A ductile shear zone within Unit I, 1 km south of the village of Philim (Fig. 2b), crops out (Pêcher & Fort, 2012).

In both valleys, the metamorphic grade increases from biotite-grade in the LHS to sillimanite+K-feldspar grade in the migmatitic part of the GHS (Fig. 2). GHS metamorphism in both areas occurred during the Eocene to Miocene (Pêcher, 1989; Coleman, 1998; Catlos *et al.* 2001; Larson *et al.* 2011; Gibson *et al.* 2016; Walters & Kohn, 2017).

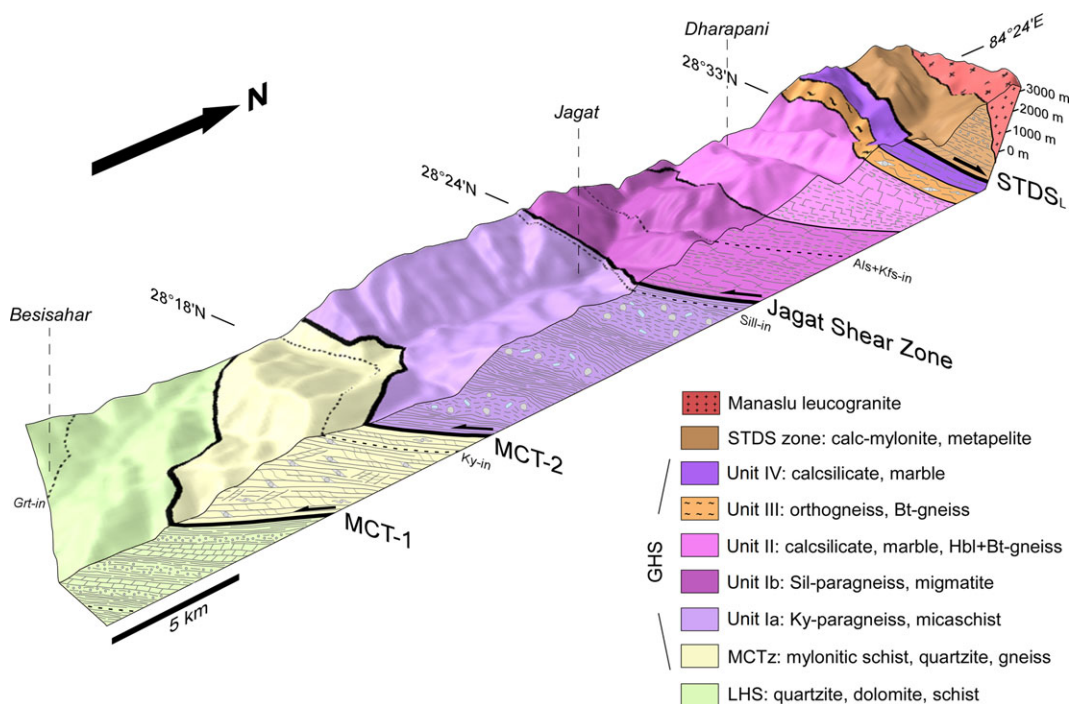


**Figure 3.** (Colour online) 3D geological model of the Marsyangdi river valley showing the location of the Jagat Shear Zone. Same legend as in Fig. 2.

### 3. The Jagat Shear Zone in the GHS

Detailed work in the Marsyangdi and Budhi Gandaki river valleys (Figs. 1, 2) resulted in the recognition and mapping of a contractional, top-to-the-S shear zone close to the sillimanite-in isograd (Figs. 2, 3) near Jagat and Philim (Figs. 2, 3). This shear zone is here referred to the Jagat Shear Zone (JSZ).

In the Marsyangdi river valley, the JSZ is a few hundred metres thick and affected garnet-aluminosilicate-bearing gneisses of Unit I. On the field, a sharp transition is discernible from tectonites showing tight to isoclinal folds and related axial plane foliation (in both the hanging wall and the footwall rocks), towards a high strain zone, showing evidences of strain localization with the developing of a mylonitic foliation and evidences of grain-size reduction. Shear planes dip to the N/NE and the associated stretching lineation plunges to the NE. Shear sense indicators (Fig. 4a–d), such as C-S fabrics, shear bands, asymmetric tails around porphyroclasts, mica and mineral fishes, asymmetric boudins and rotated garnet grains, indicate a top-to-the-S/SW sense of shear (Fig. 4a–d) pointing to a thrust-sense shear zone (Figs. 2, 4a–d). Biotite, sillimanite and minor white mica constitute the main anastomosing schistosity, wrapping around grains of feldspar, garnet and kyanite. Sillimanite is observed around garnet and kyanite oriented along the shear bands. Rare staurolite locally rims large kyanite porphyroblasts (Fig. 4e) and is microstructurally associated with sillimanite. Quartz in sheared rocks of the JSZ shows evidence of high-temperature grain boundary migration (GBM<sub>II</sub>) and recrystallization leading to chessboard extinction patterns (Fig. 4f; Kruhl, 1996; Law, 2014). Plagioclase experienced internal ductile deformation discernable by deformation twins (Fig. 4f) and asymmetric myrmekite. Deformation microstructures in the sheared rocks suggest a high-temperature deformation regime ( $T > 630\text{--}650^\circ\text{C}$ ; Kruhl, 1996; Passchier & Trouw, 2005) in agreement with the synkinematic mineral assemblage.

The JSZ separates sillimanite-garnet-bearing gneiss and migmatite (with relict kyanite) in the hanging wall (Unit Ib) from

the kyanite-garnet-rutile-bearing gneiss (Unit Ia) (Fig. 4g, h) in the footwall. In the footwall rocks, two texturally different generations of kyanite I (see also Vannay & Hodges, 1996) were observed: kyanite forms large (up to centimetre-sized) porphyroblasts (Fig. 4g) and later kyanite II occurs as small crystals along feldspar-quartz (or garnet) grain boundaries, locally associated with small euhedral staurolite (Fig. 4h). Moreover, larger anhedral staurolite (relict of prograde metamorphism) was observed, as already reported by Coleman (1998).

The JSZ crops out also in the Budhi Gandaki valley just south of Philim, where a zone of intense deformation occurs affecting garnet-aluminosilicate-bearing gneisses of Unit I. In this valley, footwall rocks are represented mainly by garnet-kyanite-bearing paragneiss, with sporadic relicts of staurolite and minor quartzite, whereas hanging wall rocks are made mostly by sillimanite-bearing migmatitic gneiss with minor calcsilicate levels. Also in this location, shear planes dip to the N/NE and the associated stretching lineation plunges to the NE. The highly deformed rocks show abundant sigmoidal quartz (Fig. 5a) and C-S fabric at the mesoscale. The spaced schistosity is defined by biotite and white mica wrapping around garnet and feldspar grains. Garnet shows an internal foliation at high angle with respect to the external schistosity. Thus, we regard garnet as an intertectonic (Passchier & Trouw, 2005) mineral. At the microscale, C-S fabric, foliation fishes and rotated garnet grains point to a top-to-the-S sense of shear (Fig. 5b). Quartz shows evidence of dynamic recrystallization through grain boundary migration (GBM<sub>II</sub>) (Stipp *et al.* 2002) with the presence of window structures. Plagioclase is ductilely deformed as indicated by the development of deformation twins. Previously, along the Budhi Gandaki valley, Parsons *et al.* (2016c) highlighted on their map S foliations and C planes in correspondence of the shear zones. Pêcher and Fort (2012) hypothesized a thrust-sense shear zone by the occurrence of high-strain levels containing sheath folds.

In order to unravel the JSZ tectono-metamorphic history, selected samples were studied to derive P-T-D-time paths. In

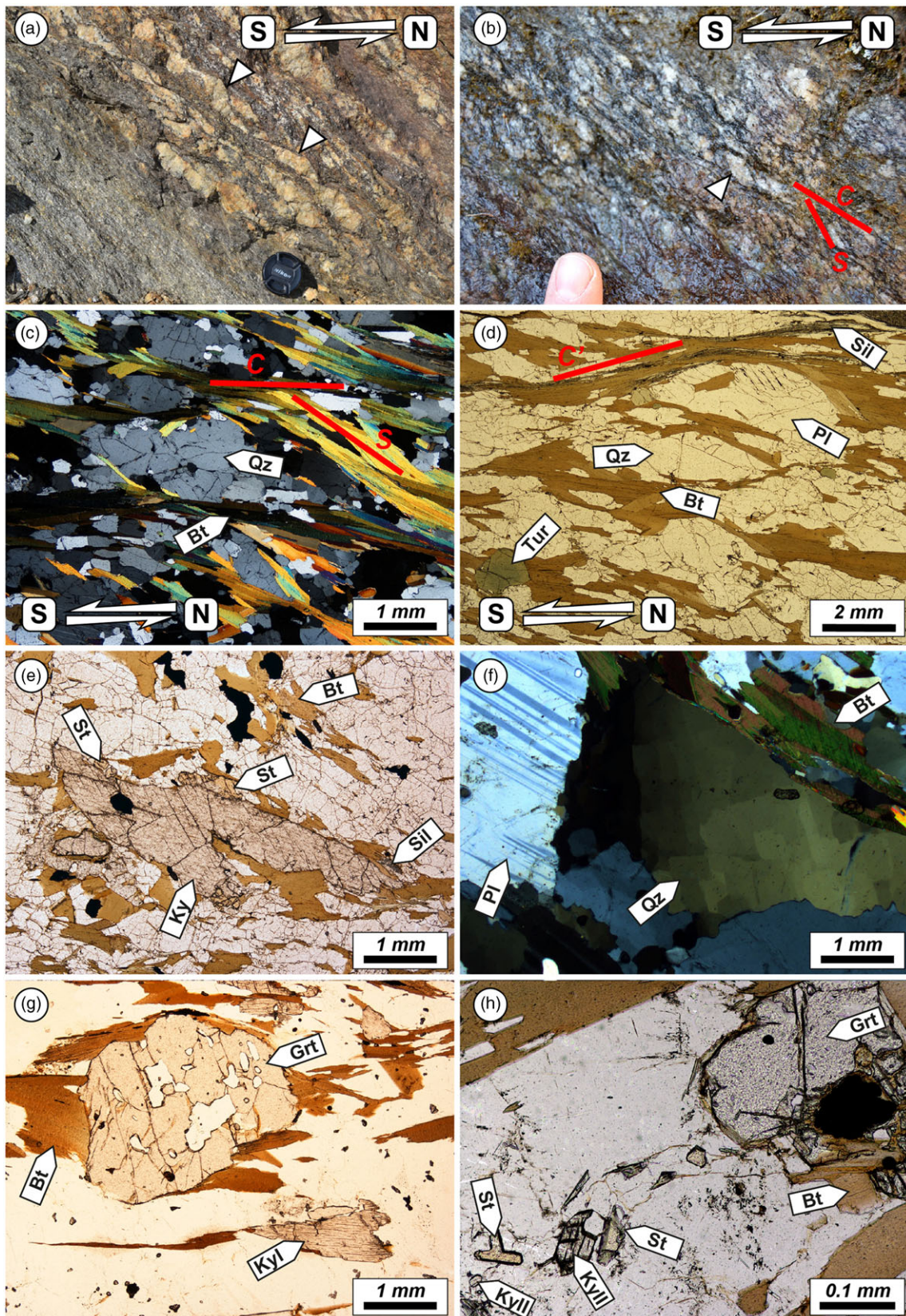


**Figure 4.** (Colour online) Meso- and microstructures of Jagat Shear Zone (JSZ) rocks and footwall rocks. JSZ: (a) Outcrop-scale sheared rocks showing quartz-feldspar sigmoidal structures (arrow) pointing to a top-to-the-S sense of shear. (b) S-C fabric and asymmetric sigmoidal quartz-feldspar lithons (arrow) in sheared garnet-aluminosilicate-bearing paragneiss, pointing to a top-to-the-S sense of shear. (c) Photomicrograph showing a S-C fabric in sheared paragneiss (crossed nicols: XPL). (d) Sillimanite-bearing shear bands in sheared paragneiss (parallel nicols, //P). (e) Large kyanite (Ky) surrounded by staurolite (St), and minor sillimanite (Sil) (//P). (f) Chessboard extinction in quartz (XPL), pointing to deformation temperatures higher than 630–650°C. Footwall of the JSZ: (g) garnet (Grt) and large Ky (i.e. Ky<sub>II</sub>) porphyroblast in paragneiss (//N). (h) Small St associated with small Ky (i.e. Ky<sub>I</sub>) within the paragneiss (//N).

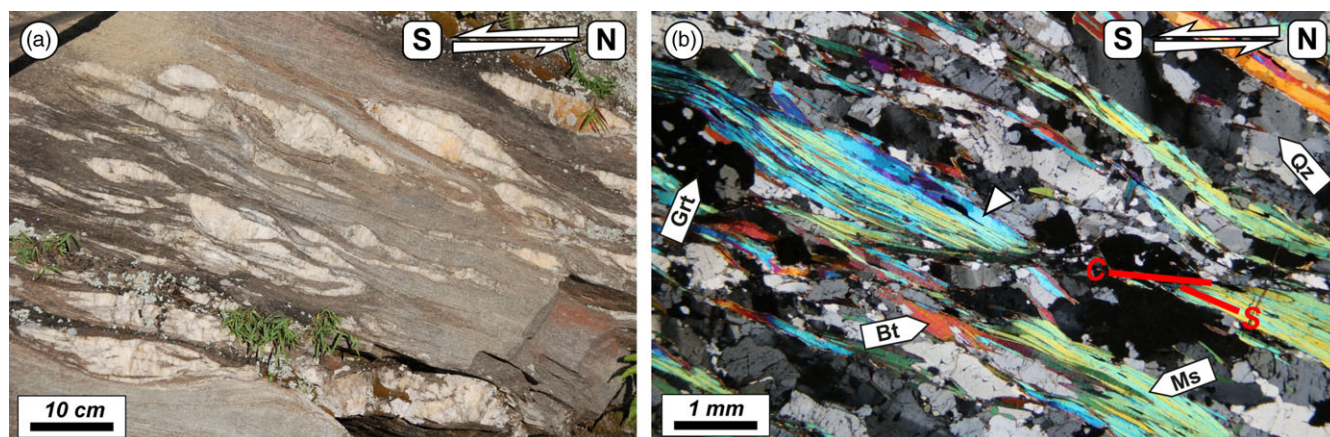


**Figure 5.** (Colour online) Meso- and microstructures of Jagat Shear Zone rocks in the Budhi Gandaki valley. (a) Sheared gneiss with quartz sigmoids and rootless folds South of the Philim village. (b) C-S fabric and foliation fish (arrow) pointing to a top-to-the-S sense of shear (XPL).

addition, a study of the petrofabrics of tectonites along the STDs profile was conducted in order to assess the Chame detachment kinematics and the relationship with the JSZ. The position of selected samples, their main assemblages and microstructural features, including the type of analyses applied, are summarized in Table 1.

#### 4. Rocks of the JSZ: mineral chemistry and geothermobarometry

Thin sections from selected field-oriented samples across a structural profile, cut perpendicular to the main foliation and parallel to the main lineation (approximating the XZ plane of the finite strain ellipsoid), were investigated using a CAMECA SX100 EMP equipped with 5 wavelength-dispersive spectrometers (WDS), hosted at the (now closed) Institut für Mineralogie und Kristallchemie (Universität Stuttgart). The energy-dispersive spectrometer of this EMP was used for qualitative identification of minerals. Synthetic and natural minerals, glasses and pure oxides were used as standards for the characterization of mineral compositions. Counting times were 20 s at the peak and on the background each. The applied accelerating voltage of 15 kV and a beam current of 30 nA and 10 nA were used to analyse garnet and other minerals (micas, feldspar, staurolite, ilmenite), respectively. Details on the analytical procedure and related errors are reported by Massonne (2012). In order to assess possible garnet zoning, multiple spots and mineral traverses were conducted together with qualitative garnet WDS X-ray elementary (for Mn, Mg, Fe, Ca and Y) maps at 60 nA with the aforementioned EMP. For analysing the Zr content in rutile, an accelerating voltage of 15 kV, a beam current of 100 nA, and 100 s counting time on peak and background each were selected. Structural formulae of minerals, and related end-member activities (used for geothermobarometry), were calculated with the A-X software (downloaded from T. Holland's personal web-page).

For geothermobarometrical estimates, a multi-equilibrium (MET) method, based on the Average P-T and Average P (at a fixed temperature) subprograms of THERMOCALC (Powell & Holland, 1994, 2008; version 3.33), was applied. Analysed garnets show slightly variable chemical zoning patterns, with flat, or nearly flat, profiles. Minor zoning in Ca was observed, and a sharp increase of Mn at the outermost rims is a common feature (see representative X-ray maps in supplementary material S1). We regard such profiles in garnet as related to diffusion modification/

homogenization due to operation of both retrograde exchange and net-transfer reactions (Kohn & Spear, 2000). Following Yakymchuk and Godin (2012), analyses of garnet with the lowest Mn (and highest Mg) contents, corresponding to mantle (or near rim) position, were combined with rim compositions of matrix minerals (not in direct contact with the garnet rim) such as micas, K-feldspar, plagioclase and staurolite (where present, see Table 1 'inferred peak mineral assemblage'). Representative mineral data are given in Table S1. For Zr-in-rutile geothermometry, the pressure sensitive calibration by Tomkins *et al.* (2007) was applied considering the pressure range of 0.7–0.9 GPa and 0.9–1.1 GPa for mylonites of the JSZ and rocks of its footwall, respectively. Only pristine rutile grains (i.e. lacking ilmenite overgrowth) in the matrix were analysed. An uncertainty of  $\pm 30^\circ\text{C}$  is assigned to the temperature estimates (Tomkins *et al.* 2007). P-T paths were derived combining microstructural and petrographic observations and P-T data from geothermobarometry with predicted mineral stability (and sequence of mineral growth) from petrogenetic grids. Metamorphic conditions for the JSZ, its hanging wall and footwall, are summarized in Table 1 and Fig. 6.

Geothermobarometric estimates suggest that JSZ mylonites equilibrated at P-T conditions of c. 0.7–0.8 GPa and c. 700°C, close to the kyanite-sillimanite boundary. Footwall rocks equilibrated at higher P of c. 1.0–1.1 GPa and lower T (<700°C) in the kyanite stability field. Hanging wall rocks returned P-T values of c. 1.1 GPa and c. 735°C, falling in the melt- and kyanite-bearing field (Fig. 6), although kyanite could be lacking in thin sections.

#### 5. *In situ* U-Th-Pb monazite petrochronology

*In situ* U-Th-Pb monazite dating was applied to obtain the timing of metamorphism and deformation along the JSZ. Microtextural position, internal features, back-scattered electron (BSE) images and chemical zoning of monazite were evaluated with the aforementioned EMP. Monazite from two selected samples (Table 1) was analysed by LASS inductively coupled plasma mass spectrometry. The analytical procedure is reported in Kylander *et al.* (2013) with modifications as reported in McKinney *et al.* (2015). U-Th/Pb and trace element data are listed in Tables S2 and S3. Representative BSE images, WDS chemical maps, spot locations and corresponding dates, are given in supplementary material S2, S3, S4 and S5. Sample MA16-90 (Fig. 2) is a mylonitic JSZ paragneiss with white and dark micas, garnet, kyanite and

**Table 1.** Summary of the main features (e.g. structural position, rock type) of selected samples (see Fig. 2 for sample locations)

Sample	GPS coordinate	Rock type	Structural position	“Peak” mineral assemblage	Comment	Method and P-T results
MC17-17	28°34'23.42"N 84°11'19.28"E	Mylonitic marble	STDS	Cal-Bt-Wm-Qz	Type II twinning in Cal	Microstructures and kinematics, CPO
MC17-02	28°32'58.1"N 84°16'55.6"E	Mylonitic gneiss	STDS	Bt-Pl-Kfs-Qz	Chessboard extinction in Qz; Feldspar fish;	Microstructures and kinematics, CPO
MA16-33	28°25'4.03"N 84°53'45.08"E	Migmatite	HW	Bt-Qz-Pl-Kfs-Grt-Sil-Ilm	Bt + Pl or Sil symplectite after Grt or Kfs (interpreted as melt consuming back-reactions); retrograde Wm and Chl	Mnz U-Th-Pb petrochronology (see main text)
MA16-86	28°27'5.20"N 84°22'23.50"E	Migmatite	HW	Bt-Qz-Pl-Kfs-Grt-Sil	Bt + Pl or Sil symplectite after Grt or Kfs (interpreted as melt consuming back-reactions); retrograde, ‘late’ Wm flakes with Sil inclusions;	AvePT: 735 (±47)°C, 1.08 (±0.15) GPa (sigfit = 1.06)
MA16-88	28°25'18.90"N 84°24'12.60"E	Mylonitic paragneiss	JSZ	Qz-Bt-Pl-Grt-Wm-Ilm-Sil	Rt inclusions in Grt; retrograde Chl	AvePT: 718 (±32)°C, 0.82 (±0.12) GPa, (sigfit = 1.06)
MA16-89	28°25'17.00"N 84°24'13.90"E	Mylonitic paragneiss	JSZ	Bt-Qz-Pl-Grt-Als-Rt-Ilm	St + Sil around Ky; Sil on Grt or Pl; retrograde Chl	Zr-in-Rt: 696–646°C (@0.9 GPa)/687–637°C (@0.7 GPa); AveP (@700°C): 0.76 (±0.08) GPa (sigfit = 1.0)
MA16-90	28°25'17.00"N 84°24'13.90"E	Mylonitic paragneiss	JSZ	Bt-Qz-Pl-Als-Grt-Ilm	Sil along C and C' planes; Sil around large Ky or Grt	Mnz U-Th-Pb petrochronology (see main text)
MA16-95	28°22'9.60"N 84°24'20.76"E	Paragneiss	FW	Bt-Pl-Qz-Grt-Ky-Ilm	Two microstructural generations of Ky: large porphyroblast (Kyl) and tiny grains (Kyll) along Grt or Pl boundaries; tiny St associated with Kyll	AveP (@680°C): 1.11 (±0.17) GPa (sigfit = 0.4)
MA16-98c	28°22'9.60"N 84°24'20.76"E	Paragneiss	FW	Bt-Qz-Grt-Ky-Rt	Chl and Rt inclusions in Grt; late retrograde Chl	Zr-in-Rt: 684–660°C (@ 1.1 GPa)/675–652°C (@ 0.9 GPa)

Minerals are listed according to decreasing modal amount.

AvePT, THERMOCALC average PT; AveP, THERMOCALC average P; FW, footwall; HW, hanging wall; JSZ, Jagat Shear Zone; STDS, South Tibetan Deattachment System; Zr-in-Rt, zirconium in rutile thermometer.

sillimanite. Sample MA16-33 is a K-feldspar-sillimanite-biotite-garnet bearing migmatitic gneiss in the hanging wall of the JSZ in the Budhi Gandaki river valley (Fig. 2), showing late white mica (as flakes and as sericite replacing sillimanite) and chlorite after biotite crystallization, likely linked to a late stage of fluid ingress and alteration.

In both samples, monazite sizes range from 30 to 200 µm in diameter. In sample MA16-90, three analysed monazite grains occur in quartz-feldspar domains: one grain is included in kyanite (Mnz 9); other grains are in biotite oriented along the mylonitic foliation. In sample MA16-33, five monazite grains are in quartz-feldspar domains and another five are hosted in mica domains. Xenotime is lacking in sample MA16-90, whereas it is observed as a rare matrix mineral in sample MA16-33. In the latter sample, in one case xenotime is in contact with high-Y monazite (Mnz 8). We would like to stress that, despite not observed, xenotime may have been present in the early-prograde stages and later on totally consumed (e.g., Pyle & Spear, 1999, 2003; Spear & Pyle, 2010).

All monazite grains are mainly concentrically zoned (Catlos, 2013), with minor patchy and oscillatory zoning in sample MA16-33 (Supplementary material S4, S5), with respect to Y, Th and heavy rare-earth elements (HREE). Cores are enriched in Th and

variably depleted in Y and HREE, whereas the rims and mantles are enriched in Y and HREE and depleted in Th (Fig. 7). Interestingly, in sample MA16-33, high-Y and HREE rim domains correspond (in some circumstances) to portions where oscillatory zoning in Th is present (Fig. 7, Supplementary material S4, S5), a feature interpreted as linked to melt-crystallization (Rubatto *et al.* 2013) during cooling. Moreover, in this sample low- to moderate-Y and HREE monazite overgrowth, as discontinuous outermost rims or forming patchy domains, are sometimes observed.

There is a good correlation between <sup>208</sup>Pb/<sup>232</sup>Th dates, Y content and Gd/Yb ratio. The dates of low-Y (and HREE) and high Gd/Yb cores range from 31 to 27 Ma, whereas high-Y and low Gd/Yb rims yielded dates between 27 and 13 Ma in sample MA16-90 (Figs. 7, 8, Supplementary material S2, S3). In sample MA16-33, we observed in part similar trends of Y, HREE and Gd/Yb in monazite. Monazite cores yielded dates from 39 to 29 Ma; rims and mantles gave dates from 28 Ma to 13–10 Ma. The older group of dates (39–29 Ma) are linked to domains with low-Y and HREE and higher Gd/Yb values (Fig. 7). The younger group of dates shows more complicated trends. An increase in Y and HREE, together with a decreasing in Gd/Yb, is observed until ~17–15 Ma, whereas youngest dates (13–10 MA) are associated together with decrease in Y (and HREE) and variable to increasing Gd/Yb values.



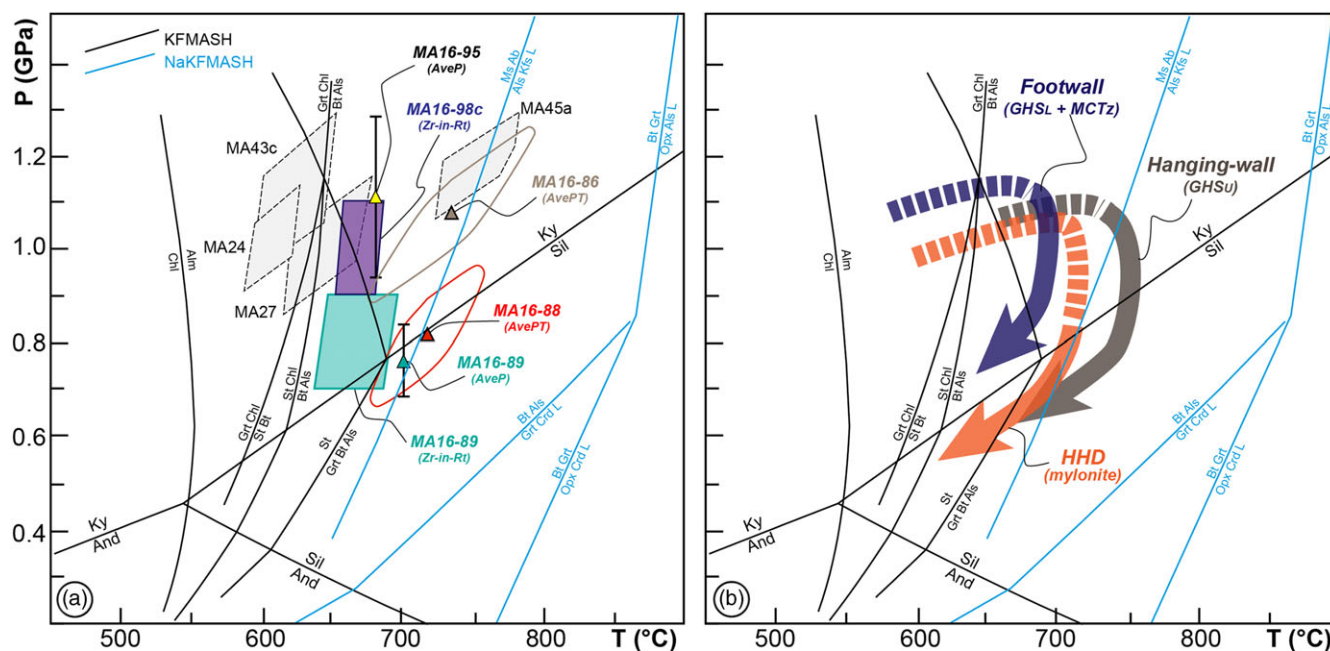


**Figure 6.** (Colour online) (a) P-T results of selected samples taken from different structural positions along the studied transect. Grey boxes refer to P-T estimates given in Catlos *et al.* (2001) (see Table 1 and main text for details, Fig. 2 for sample location). KFMASH equilibria plotted with the GIBBS software (Spear & Menard 1989) using the SPaC2007 database. NKFMASH curves are after Spear *et al.* (1999). (b) Reconstructed P-T paths of different GHS portions, based on geothermobarometry and petrographic observations.

Due to the good correlation among dates and monazite chemical composition, we interpret the obtained dates as follows according to Kohn *et al.* (2005), Braden *et al.* (2017) and Soucy La Roche *et al.* (2018). Interpretation of the Y and HREE zoning in monazite rely on the observation assumptions that garnet is the main silicate controlling the budget of these elements during metamorphisms (Pyle & Spear, 1999, 2003; Gibson *et al.* 2004; Kohn *et al.* 2005; Pyle & Pyle, 2010 and references therein).

The low-Y, high-Th and high Gd/Yb monazite cores are linked to the prograde burial path and formed contemporaneously with garnet, starting at 39 Ma (a minimum age) and ceasing at 28–27 Ma. It is worth noting that the span of time ~ 29–27 Ma is retrieved also from monazite (Mnz 9) hosted in kyanite in sample MA16-90, showing intermediate Y contents (Fig. 7). The chronological interpretation of such a grain is tricky. Indeed, Gibson *et al.* (2004) reported the possible formation of coeval kyanite and monazite, with intermediate Y content (see their reaction 4), around peak pressure along a prograde clockwise P-T path.

On the contrary, Soucy La Roche *et al.* (2022) demonstrated that monazite inclusions in kyanite may form on the retrograde path during the partial replacement of kyanite by white mica based on the observation that monazite intersects fractures filled with white mica, which could have served as fluid pathways. We documented cracks in kyanite around hosted monazite, but there is no white mica or other evidence for late replacement of kyanite or fluid infiltration; therefore, we interpret the 29–27 Ma Mnz 9 as a primary inclusion that constrains the timing of peak P conditions.

High-Y and low Gd/Yb monazite rims crystallized along the decompression and retrograde path, where the breakdown of garnet to mica and sillimanite and melt crystallization in the migmatite (MA16-33) occurred in the time span of 28–27 Ma down to 13 Ma. Matrix monazite (Mnz 8) in MA16-33 is interpreted to have co-crystallized at 19–14 Ma with xenotime that

may have formed due to garnet breakdown (Spear *et al.* 1999; Gibson *et al.* 2004; Spear & Pyle, 2010). The youngest group of ages (down to 10 Ma), in light of their different more variable chemistry, and lack of clear chemical trends are interpreted as related to late, locally, fluid-mediated monazite alteration/recrystallization (Kohn *et al.* 2005).

## 6. Chame detachment: petrofabric data

In order to determine the kinematics of the Chame detachment, which is crucial for any tectonic interpretation of the southernmost JSZ, tectonite samples were characterized and compared with rocks from a strand of the STDS, the Phu detachment, which occurs in the northern Marsyangdi river valley (see Table 1, Figs. 2a, 9). Microstructures, integrated with field observations, were investigated with standard polarization microscopy. Calcite and quartz crystallographic preferred orientations (CPO) were studied at the Geowissenschaftliches Zentrum Göttingen through an X-ray Texture Goniometer (X'Pert Pro MRD\_DY2139 by PANalytical). X-ray texture analyses were performed on areas of ~ 3 cm<sup>2</sup> in rock slices (~1 cm thick) cut parallel to the XZ and YZ planes of the finite strain ellipsoid. For each sample, crystallographic orientation data from both planes were combined to recalculate the Orientation Distribution Function through MTEX Toolbox (available for download at: <https://mtex-toolbox.github.io/>) of the Matlab software. The adopted lattice parameters were: a = b = 4.913 Å, c = 5.405 Å for quartz and a = b = 4.988 Å, c = 17.062 Å for calcite. As both mineral phases are trigonal, crystal symmetry '312' (limited to Laue groups) was adopted. The main crystallographic directions of quartz and calcite were displayed on equal area lower hemisphere pole figures with a projection plane normal to the foliation and parallel to the lineation, using the kernel de la Vallée Poussin function (Schaeben, 1997) with a halfwidth of 10° (Hielscher & Schaeben, 2008).

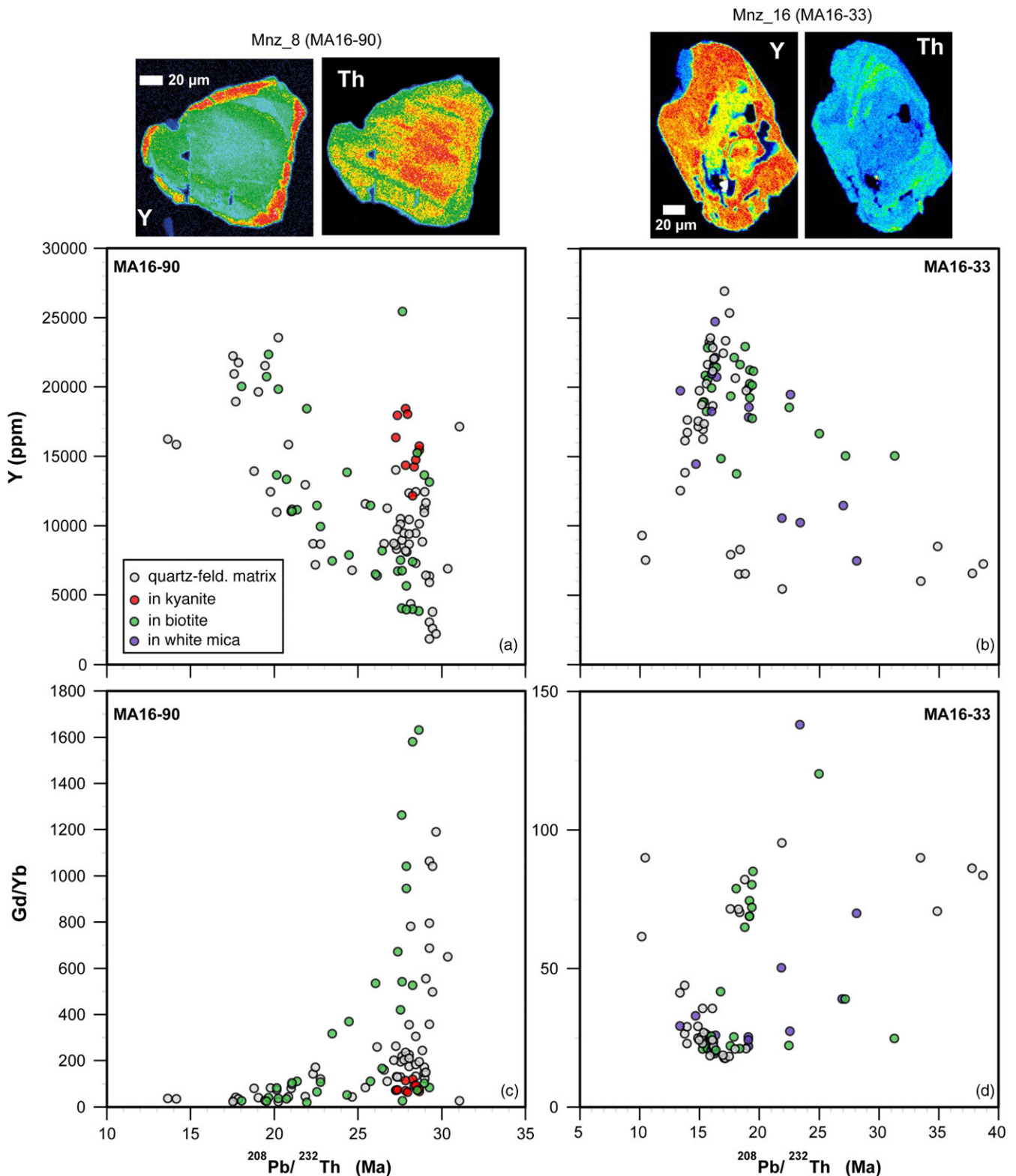


**Figure 7.** (Colour online) Monazite petrochronological results from sample MA16-90 and MA16-33. Plot of Y (ppm) vs.  $^{208}\text{Pb}/^{232}\text{Th}$  dates (a) sample MA16-90 (b) sample MA16-33. Plot of Gd/Yb ratio vs.  $^{208}\text{Pb}/^{232}\text{Th}$  ages (c) sample MA16-90 (d) sample MA16-33. Representative compositional maps (Y and Th) of monazites from both samples are included in the upper part of the figure. Warm colours point to higher concentration.

At the outcrop-scale, mica fishes and rotated mantled porphyroclasts, in sheared leucogranite (Fig. 9a, b), indicate a top-down-to-the-NW sense of shear that is cryptic at the microscale. We selected two samples (MC17-02 and MC17-17)

for CPO analyses. Sample MC17-02 is a sheared gneiss (Fig. 2) and sample MC17-17 a marble (Fig. 2) collected at the Chame detachment and in the footwall of the Phu detachment (near the village of Brathang), respectively. Sample MC17-02 (Fig. 9c) shows

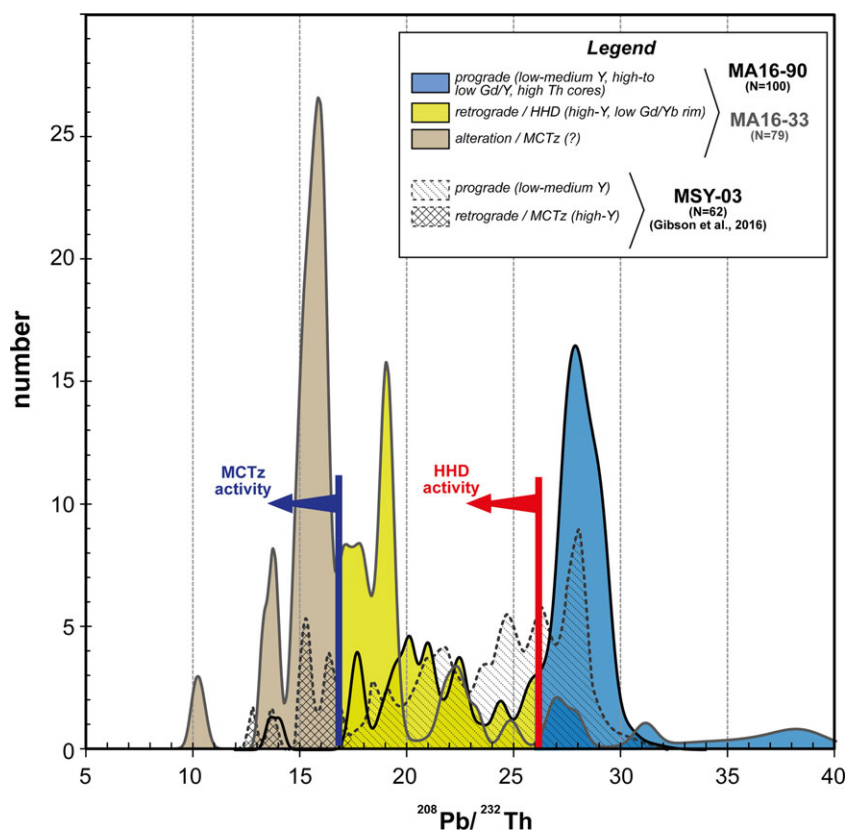


**Figure 8.** (Colour online) Histogram of  $^{208}\text{Pb}/^{232}\text{Th}$  dates vs. number of analyses for samples MA16-90, MA16-33 (this study), and MSY-03 (Gibson *et al.* 2016) with arrows marking prograde and retrograde evolutions according to chemical zoning of monazite and age of the HHD (Jagat Shear Zone) and Main Central Thrust (MCT).

a heterogeneous mineral distribution, where shape preferred orientation (SPO) of biotite and plastically deformed quartz and feldspar define a spaced foliation.

Quartz CPO patterns (Fig. 9e) show a mid-low CPO intensity, displayed by a classic ‘texture index’ of 1.6 (Bunge, 1982) and a M-Index of 0.01 (designed for large ODF datasets, Skemer *et al.* 2005). Quartz [c]-axis maxima (on [0001] pole figure), between the Z- and X-directions of the finite strain ellipsoid, are consistent with type I cross girdle with a fabric opening angle fabric of ca. 72°, corresponding to a deformation temperature of  $\sim 580^\circ \pm 50^\circ\text{C}$  (Law, 2014). The asymmetric pattern suggests a non-coaxial flow (Lister & Hobbs, 1980; Wallis, 1992; Law & Johnson, 2010). Dextral asymmetry of [c]-axis maxima, compared to the geographical reference system, is coherent with a top-to-the-N non-coaxial deformation.

Marble MC17-17 (Fig. 9d) shows a rough continuous foliation defined by a SPO of fine-grained biotite and slightly elongated calcite. Calcite is well-interconnected, representing the weak matrix (Handy, 1994). Lobate grain boundaries and unimodal distribution indicate a grain boundary mobility mechanism (GBM regime) (Fig. 9d). Type II e-twins, typical for temperatures below 300 °C (Burkhard, 1993; Ferrill *et al.* 2004), occur. A texture index of 1.2 (Bunge, 1982), consistent with a M-Index of 0.03, supports a mid-CPO intensity (Skemer *et al.* 2005) for calcite. Well-defined patterns and asymmetric sinistral [c]-axis maxima in the Z-direction, with further maxima on Y-direction (central girdle), are recognized (Fig. 9e). Sinistral asymmetric poles to the {e}-planes (on {0118} pole figure) support {e}-twinning development in a top-to-the-N non-coaxial flow (Fig. 9e). The {r}-planes maxima (on {1014}) and the {f}-planes (on {0112}) define small circles, coherent with the coexistence of intracrystalline deformation. Intracrystalline slip and twinning support a deformation temperature range of 300–800 °C (De Bresser & Spiers, 1997).

According to the c-axis-based method of Wenk *et al.* (1987), calcite asymmetric texture (of ca. 7°) results from a general flow with low simple shear contribution (~26%).

## 7. Discussion

### 7.a. JSZ: P-T-D-t path and implications

The *in situ* U-Th-Pb dating of zoned monazite in rocks from the Marsyangdi and Budhi Gandaki valleys yielded dates from ~ 39 to 13 Ma (Fig. 8). Similar dates have been obtained by Coleman (1998), Catlos *et al.* (2001, 2018), Gibson *et al.* (2016) and Larson *et al.* (2011) highlighting younger dates from north to south. The zoned monazite studied in this work allowed us to better unravel the metamorphic and deformation history. Chemical zoning and LASS results indicate that the older monazite dates are related to prograde metamorphism between 39 and 28–27 Ma, whereas the younger dates, obtained from high-Y and HREE rims, constrain the start of the retrograde path at 28–27 Ma. This path recorded by rocks from the hanging wall of the JSZ is a result of the reverse kinematics of the shear zone forcing the hanging wall rocks to move upward and southward. The youngest monazite ages suggest that in a time interval lasting 11–10 My (from 28 Ma to 17 Ma) the footwall of the shear zone moved downward while the hanging wall was simultaneously moved upward and exhumed. The hanging wall underwent retrograde metamorphism and exhumation over a duration of 11–10 My before the movement of the footwall started.

The occurrence of the thrust-sense, top-to-the-S shear zone, located at the boundary between sillimanite-bearing gneiss and underlying kyanite-bearing rocks, as well as the timing of this zone is in agreement with the structural position and age of the HHD determined by Montomoli *et al.* (2013, 2015) and Iaccarino

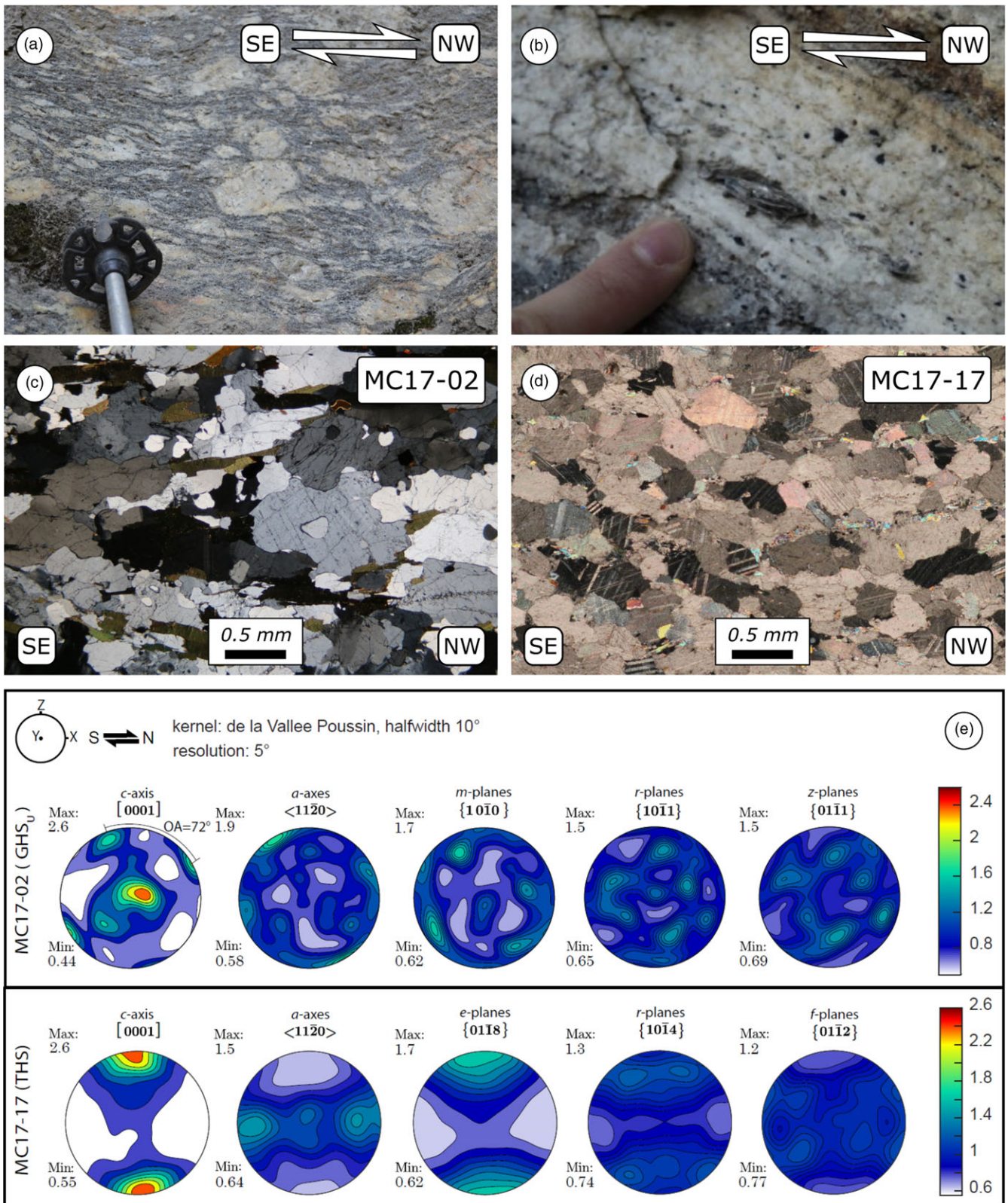


**Figure 9.** (Colour online) Mesoscopic kinematic indicators of the Chame detachment: a) delta-type porphyroclast in orthogneiss in the uppermost part of the GHS; top-down-to-the-NW sense of shear; b) mica fish in sheared leucogranite; top-down-to-the-NW sense of shear. c) Photomicrograph of sample MC17-02 (deformed gneiss); foliation is highlighted by biotite and shape preferred orientation (SPO) of both feldspar and quartz (XPL); d) photomicrograph of sample MC17-17 (XPL), a pure marble with a grain SPO; e) equal area lower hemisphere pole figures of the main crystallographic elements for quartz and calcite textures in samples MC17-02 and MC17-17 (upper and lower row, respectively).

*et al.* (2017a) in Western Nepal, Iaccarino *et al.* (2015) and Wang *et al.* (2015, 2016) in Central Nepal, Chakraborty *et al.* (2019) and Benetti *et al.* (2021) in India and Waters (2019) in Nepal. Metamorphic conditions of selected samples are consistent (Fig. 6) with both the inferred 'peak' mineral assemblage (and related mineral stability constrained from petrogenetic grids) and previous estimates by Coleman (1998) and Catlos *et al.* (2001). Only the hanging wall sample (MA16-86), containing sillimanite, plots in the kyanite stability field. This could be due to the lack of equilibration, the determination of P-T conditions from mineral that formed/equilibrated prior to the decompression and/or the difficulty to consider P-T errors (here:  $\pm 0.1$  GPa,  $\pm 30^\circ\text{C}$ , see parag. 4) adequately. We note that our derived P-T conditions are consistent with P-T data of calcsilicates collected just above MA16-86 (see Walters & Kohn, 2017). Therefore, we favour the first explanation 'P-T conditions prior to the decompression'. Our kinematics and P-T-D-t path of the JSZ are in agreement with data on the HHD in nearby areas such as the Kali Gandaki valley (Iaccarino *et al.* 2015). As a consequence, the occurrence of the JSZ in the Manaslu massif fills a gap in tracing the HHD to the east, confirming its regional extent.

### 7.b. How is strain accommodated in the HHD?

The occurrence of a regional scale HHD in the GHS showing a thickness ranging from a few dozens of metres up to nearly 4 km poses a problem if it is a single shear zone or a wide zone of deformation concentrated at several shear zones acting at different times. Montomoli *et al.* (2013, 2015) firstly documented the occurrence of the HHD between 28 and 17 Ma by the presence of sheared rocks, kinematic indicators, geothermobarometry on hanging wall and footwall rocks and U-Th-Pb *in situ* dating of monazite. In Western Nepal, the shear zone is characterized by thick mylonites (up to 4 km; Montomoli *et al.* 2013; Iaccarino *et al.* 2017a). U-Th-Pb dating on monazite yielded a relatively wide time span of shearing from 28 to 17 Ma.

In Central Nepal, Shrestha *et al.* (2020) using detailed petrochronology on rocks from both the Banuwa and Sinuwa thrusts were able to document the occurrence of two main in-sequence thrust-sense shear zones active within the time span of the activity of the HHD: starting at  $\sim 24$  Ma for the Sinuwa thrust and  $\sim 21$  Ma for the lower Banuwa thrust. However, the kinematics of the Sinuwa thrust is only inferred, whereas the kinematics of the Banuwa thrust is still under discussion: Martin *et al.* (2010, 2015) proposed normal-sense kinematics, whereas Corrie and Kohn (2011) suggested a thrust-sense kinematics active from 27 to 22 Ma. Shrestha *et al.* (2020) proposed an initial thrust-sense, top-to-the-S Banuwa thrust, which was later re-activated as a normal-sense, top-down-to-the-N, shear zone (at  $\sim 10$  Ma).

In NE Nepal, Ambrose *et al.* (2015) proposed the occurrence of five 'cryptic' shear zones in the GHS and out of sequence thrusts, indirectly detected on the basis of integrated pseudosection modelling and monazite petrochronology of paragneiss, active from 31 to 12 Ma, mostly falling within the timing of the HHD. However, both the occurrence and the kinematics of the 'cryptic' shear zones were only inferred. In addition, they often lack direct evidence of strain localization (high strain zones) such as mylonites or sheared rocks and related meso- and microscale kinematic indicators.

Eastern Nepal is characterized by a major number of (inferred) metamorphic discontinuities with respect to Western and Central Nepal (Cottle *et al.* 2015; Larson *et al.* 2015) where one or two

tectono-metamorphic discontinuities have been documented so far (Carosi *et al.* 2016, 2018) on the basis of structural and field observations in addition to petrological and geochronological data.

The GHS was affected by polyphase tectonics with several generations of folds, foliations and intra-GHS discontinuities so that much caution is requested in attributing a tectonic significance and, moreover, a kinematics of samples showing different P-T data without the help of field evidences and structural analysis.

However, the occurrence of several metamorphic discontinuities in the GHS, if further confirmed on structural basis, does not prevent the occurrence of a major HHD between sillimanite-bearing migmatites, with a higher degree of melting, and kyanite-bearing gneiss below (Montomoli *et al.* 2013, 2015).

Further investigations are required to better understand if the HHD is a unique shear zone or if it is made of several (in-sequence?) shear zones and what type of shear zone the HHD is (Type I, II, III and IV *sensu* Fossen & Cavalcante, 2017). This latter point is particularly interesting (to be the target of future research), since it would allow to better understand how strain is distributed within large, regional scale, shear zones affecting medium- to high-grade metamorphic rocks. As suggested by Montomoli *et al.* (2013), it is necessary to perform detailed meso- and micro-structural analyses on mylonites or sheared rocks combined with detailed thermobarometry of the hanging wall and footwall rocks as well as petrochronology in order to be able to discriminate real ages of shearing in the wide time span of 28–17 Ma. However, to exclude possible ambiguities in the interpretations, we would like to stress that shear zones and their sense of shear should be recognized at the meso- and micro-scale by structural analysis and not only inferred by differences in P-T conditions or ages.

### 7.c. The Chame detachment

Walters and Kohn (2017) identified a strand of the HHD in the upper part of the Marsyangdi valley interpreting the Chame detachment (Coleman, 1998) as a thrust-sense shear zone and a lateral-ramp of the HHD (Fig. 1). However, new data, at a different scale (Fig. 9), allowed us to evaluate kinematic indicators. Both mesoscopic kinematic indicators (e.g. mica fish in the leucogranite and delta-type porphyroclast in orthogneiss in the uppermost part of the GHS, Fig. 9a, b) and asymmetric quartz textures in gneiss (Fig. 9e) suggest that the Chame detachment deformed the orthogneiss and the leucogranite through a non-coaxial flow with a top-down-to-the-N normal-sense of shear. The same kinematics is constrained for the marbles affected by the Phu detachment (Fig. 9e). Therefore, the Chame detachment cannot be directly identified as a strand of the HHD, as far as its entire activity is concerned.

Indeed, considering that the CPOs obtained for both the Chame and the Phu detachments depend on the strain memory of quartz and calcite (i.e. it is not possible to state without doubt that they reflect the entire deformation history of the tectonic discontinuity rather than a part of the plastic history), the Chame detachment can be still interpreted as an early thrust-sense shear zone later reactivated as a normal-sense shear zone, with a full re-orientation of the quartz crystal lattice and a transposition of the kinematic indicators. It is worthy of note that a comparable tectonic history, with a switch in the kinematics, was also proposed for the Annapurna detachment in the nearby Kali Gandaki valley (Vannay & Hodges, 1996). In the broad time span of the HHD activity (28–17 Ma), the deformation was likely localized at different levels complicated by the presence of thrust and lateral ramp or migrated

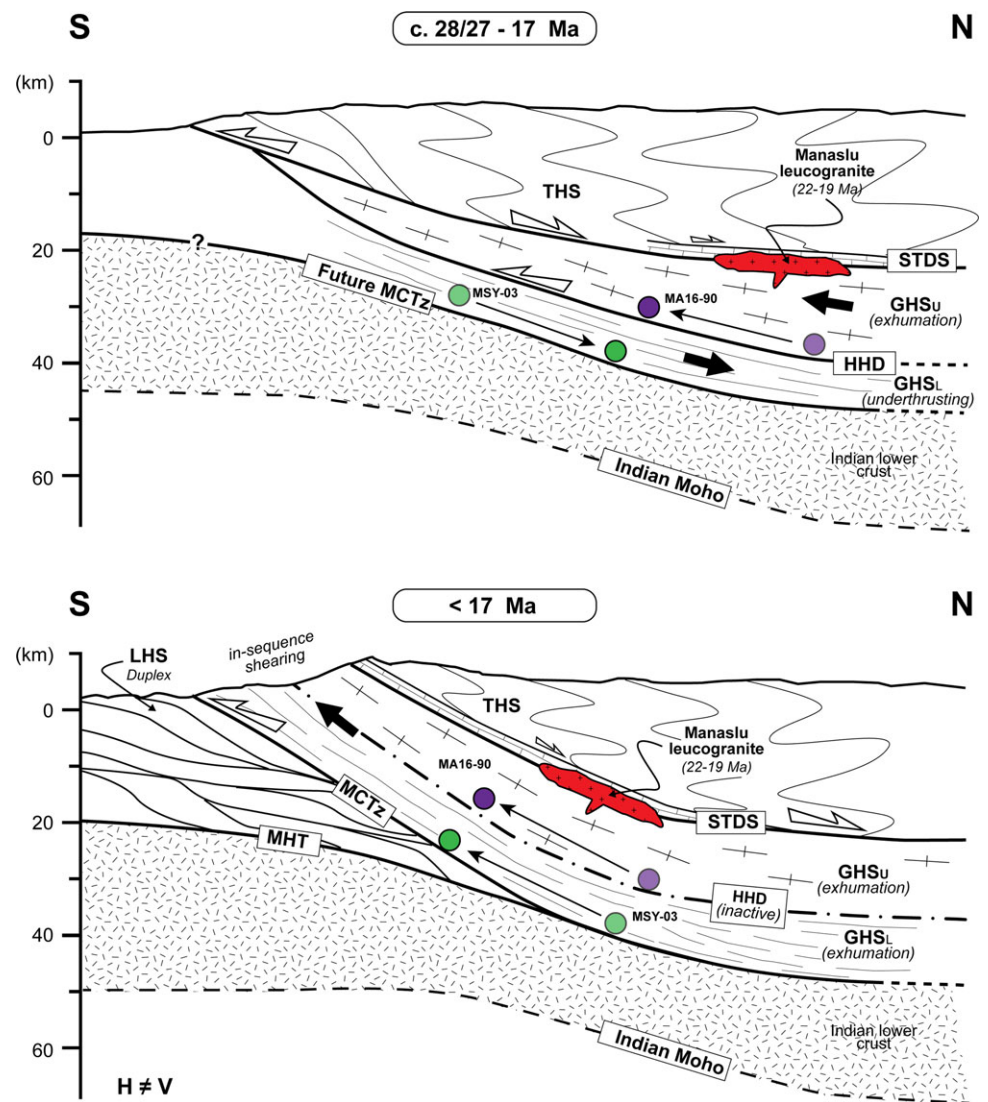


**Figure 10.** (Colour online) Sketch of the tectonic evolution on the Greater Himalayan Sequence in the Marsyangdy and Budhi Gandaki river valleys at 28–27 Ma, the time of activation of the Jagat Shear Zone (HHD) (upper) and at 17 Ma, the time of activation of the Main Central Thrust zone (MCTz) (lower). Violet and green dots are reported at depths appropriate for available P–T data.

from north to south. Potentially, it is a first thrust-sense shear zone localized (upper HHD) close (or coincident) to the ‘current’ Chame detachment and then migrated some kilometres downward to the level of the JSZ. This is in agreement with the occurrence of higher and older shear zones in the upper part of the GHS such as the Kalopani shear zone in the Kali Gandaki valley active between 41 and 28 Ma (Carosi *et al.* 2016).

The later reactivation as a normal sense shear zone in the upper GHS (Chame detachment) could be a tectonic event of the orogenic prism in response to the thickening of the GHS caused by the thrust-sense motion of crustal slices of the GHS along the HHD. The occurrence of a normal sense shear zone at the top of the GHS, assisted by erosion, could explain the exhumation of the GHS between the Chame detachment and the HHD.

#### 7.d. Shifting of deformation from the HHD to the MCT

Movements along the JSZ, correlated with the HHD, from 28–27 to 17 Ma caused a discontinuity in the metamorphic paths of the hanging wall and footwall rocks (Fig. 10). Until 28–27 Ma, these rocks experienced prograde burial, but after the activation of the HHD a remarkable difference in the timing of exhumation was

introduced (Figs. 8, 10) with the hanging wall exhumed 11–10 My earlier than the footwall. In this sense, P–T paths of rocks across the GHS alone are similar and not sufficient to recognize or to locate the HHD or other tectono-metamorphic discontinuities without studying kinematics and petrochronology.

Sample MSY-03, studied by Gibson *et al.* (2016), is located in the footwall of the JSZ and in the hanging wall of the MCT (Fig. 2a) and constrains, with *in situ* U–Th–Pb analyses on monazite, prograde metamorphism between 31 and 17 Ma and retrograde metamorphism from 17 to 13 Ma, that is, nearly 10 My later than the cooling and exhumation of the hanging wall of the JSZ. According to Catlos *et al.* (2001), the mapped metamorphic isograds are not displaced and the monazite ages decrease with no break from the JSZ to the MCT zone (from 22 to 15 Ma). In addition, no discontinuities have been detected in the field from the JSZ to the MCT so, even if the occurrence of minor ‘cryptic’ discontinuities cannot be ruled out, we regard the sample MSY-03 as representative of the behaviour of the footwall of the JSZ as a whole without the occurrence of major discontinuities. The retrograde ages between 17 and 13–10 Ma recorded in the monazite of rocks from the footwall (sample from Gibson *et al.* 2016) and hanging wall of the HHD could be caused by the

recrystallization/alteration (?) linked to the MCT (Fig. 10). This is in agreement with the ages of the HHD and MCT in Montomoli *et al.* (2013), who demonstrated that deformation shifted in space and time from the HHD to the lower MCT at ~ 17 Ma, and Carosi *et al.* (2010), who found that HHD shearing ceased at 17 Ma in Western Nepal. Since the position of the MCT is still under debate, spanning for dozens of kilometres, from the chlorite isograd in the LHS up to sillimanite isograd in the GHS along the Himalayan belt (Searle *et al.* 2008; Martin, 2017b; Carosi *et al.* 2018) the precise identification and timing of HHD, MCT and shear zones in the upper LHS is necessary to unambiguously locate the MCT in different sections of the belt. Fixing the tectonic boundaries of the GHS and their timing is a fundamental step towards a meaningful identification of the assembly and the exhumation mechanisms of the GHS (Kohn, 2008; Carosi *et al.* 2010, 2013; Corrie & Kohn, 2011; Montomoli *et al.* 2013, 2015; Montemagni *et al.* 2020; Benetti *et al.* 2021).

To unambiguously distinguish between the HHD and MCT, it is necessary to integrate structural, metamorphic and geochronological investigations in sections perpendicular to the strike of the belt. The identification and timing of the HHD and MCT constrained in such sections help to better identify the position and age of the MCT, a still debated topic in the Himalayan geology since the last century. In this way, the lower limit of the GHS can be traced.

### 7.e. Correlation of samples in regional scale shear zones

The Himalayan belt offers the opportunity to directly observe large-scale shear zones both along strike and parallel to the tectonic transport for hundreds of kilometres. Braden *et al.* (2020), who studied two sections of the MCTz from an external klippe to the inner part of the orogenic belt in Western Nepal, found that these sections of the MCTz record different ages of shearing: they are older in the external klippen and younger in the inner portion of the GHS. This led to the interpretation of the occurrence of an out of sequence MCTz in the inner GHS.

Considering the four types of shear zones described by Fossen and Cavalcante (2017), except type III that maintains a constant thickness, the active shearing migrates through time towards the inner (core) or towards the external part (wall rocks) of the shear zone depending on the shear zone type. To avoid possible misinterpretations in correlating samples in large-scale regional shear zones, we need to know the geometry, kinematics and evolution type of the investigated shear zone. Therefore, great care should be taken when correlating few samples over long distances because, for example, a younging age from one place to another could be only apparent without the knowledge of the shear zone type.

The framework is complicated by the fact that the same large-scale shear zone (e.g. HHD or equivalents) in a single section shows rejuvenation ages from the upper part to the lower part as documented by detailed petrochronological studies on the Sinuwa and Banuwa thrusts in Central Nepal by Shrestha *et al.* (2020). The same happens at a larger scale when considering the position and age of the Kalopani shear zone (Carosi *et al.* 2016), the HHD (Montomoli *et al.* 2013; Carosi *et al.* 2018) within the GHS, and the MCT (Montomoli *et al.* 2015; Benetti *et al.* 2021). So, the problem of a regional and long-lasting shear zone is a 3D problem plus time, for which many data are necessary. In addition to this, Roberts *et al.* (2020) found a syn-orogenic rotation of the MCT in Sikkim, not detected in other sections of the belt. In this case, we should

compare geochronological data considering the changing attitude of the stretching lineation.

By considering shear zones occurring in the same vertical section perpendicular to the belt, we can reasonably compare the age of shearing and the kinematics. Much caution is necessary when comparing samples collected along the tectonic transport over long distances, especially in the frontal part of the belt where the GHS is progressively thinned to the point where the THS meets the LHS (Webb *et al.* 2007). When the GHS is tectonically thinned by components of both pure shear and simple shear during ongoing deformation (Long & Kohn, 2020), shear zones within it could be 'telescoped' and the correlation of samples over dozens or hundreds of kilometres can be very difficult so that great caution is needed in their interpretation.

The problem could be overcome by applying a multidisciplinary approach taking into account structural data at the meso- and microscale, P-T estimations and petrochronology, to compare samples collected along different sections. A similar problem is the comparison of shear zones along the strike of arcuate belts. Such belts could be caused by different amounts of displacement along thrusts or affected by inherited lateral discontinuities, striking perpendicular with respect to the main structural trend of the belt and the shear zones (Gibson *et al.* 2016; Soucy La Roche & Godin, 2019). In this way, two Himalayan sections, along the same parallel, could record different ages of southward propagation of the thrust-sense shear zone.

## 8. Conclusion

Geological investigations in the Marsyangdi and Budhi Gandaki river valleys allowed us to detect and to map, on a structural basis, a previously unrecognized ductile shear zone (JSZ) in the GHS, separating sillimanite-garnet bearing gneiss from lower kyanite-garnet bearing gneiss. It is a thrust-sense shear zone with a top-to-the-S sense of shear. The JSZ sheared rocks equilibrated at P-T conditions of ~ 0.7–0.8 GPa and nearly 700°C, whereas footwall rocks equilibrated at higher P of ~ 1.0–1.1 GPa and a  $T < 700^\circ\text{C}$ . *In situ* U-Th-Pb dating on texturally controlled and chemically zoned monazite allowed us to constrain the age of ductile shearing between 28 and 17 Ma. The activity of the JSZ caused the earlier exhumation of its hanging wall joined to the activity of the Chame detachment (a lower strand of the STDS) and/or erosion and tectonic thinning due to the pure shear component of non-coaxial deformation in the GHS. These features confirm that the JSZ is the along-strike continuation of the HHD in Central Nepal and demonstrate the regional extent of the HHD in the Himalayan orogenic belt. To better understand its architecture and evolution, further detailed studies are necessary by integrating structural investigations on sheared rocks, P-T data and detailed petrochronology in sections perpendicular to the grain of the belt.

Detailed structural investigation by meso- and microscale kinematic indicators joined to quartz and calcite CPOs in the Chame detachment and a further strand of the STDS confirmed its extensional, top-to-the-NE kinematics. It firstly acted as a thrust (Walters & Kohn, 2017) in the upper portion of the Greater Himalayan Sequence and then was re-activated as a detachment in response to the motion of the HHD causing an overthickening in the GHS and subsequent exhumation of the hanging wall rocks of the HHD.

The HHD and MCTz are two distinct shear zones in the middle and lower GHS which were active at different times within the MCTz marking the lower boundary of the Himalayan

metamorphic core. The upper limit of the metamorphic core in the study area is the Chame detachment acting as a normal-sense shear zone (i.e. the local strand of the STDS). Exhumation of the GHS was accomplished by in-sequence shearing with first activation of the HHD (28–17 Ma) and later activation of the MCTz (17–13–10 Ma) at a lower structural position. Precisely determining the boundaries of the metamorphic core, investigating structures within the core and determining the timing of shearing on the boundaries will allow us to better unravel the tectonic evolution and exhumation history of the Himalayan core.

**Supplementary material.** The supplementary material for this article can be found at <https://doi.org/10.1017/S0016756823000365>

**Acknowledgements.** Research funded by PRIN 2015 (University of Torino: R. Carosi and C. Montomoli), funds Ricerca Locale University of Torino (ex-60%, S. Iaccarino and C. Montomoli) and University of California funds (J. Cottle). We are grateful to A. Pêcher and S. Guillot for the fruitful discussions on the geology of the Manaslu massif, to B. Leiss for the support with the XTG, to T. Theye for the support with EMP and to G. Tartaglia for helping with part of the geochronological analysis.

We thank R. D. Law, M.P. Searle and R. Soucy La Roche for their comments and revisions that greatly helped to improve the quality of this paper. We also thank the Editor O. Lacombe for handling this paper.

**Author contributions.** RC and CM: field work, sampling, formal analysis, methodology conceptualization, writing, project administration and funding acquisition; SI: field work, sampling, formal analysis, methodology, conceptualization, writing and funding acquisition; JC: formal analysis, methodology, writing and funding acquisition; HJM, LN and MS: formal analysis, methodology and writing.

**Competing interests.** None.

## References

- Agustsson KM, Gordon SM, Long SP, Seward GGE, Zeiger K and Penfold M (2016) Pressure-temperature-structural distance relationships within Greater Himalayan rocks in eastern Bhutan: implications for emplacement models. *Journal of Metamorphic Geology* **34**, 641–62.
- Ahmad T, Harris N, Bickle M, Chapman H, Bunbory J and Prince C (2000) Isotopic constraints on the structural relationship between the Lesser Himalayan Series and the High Himalayan Crystalline Series, Garhwal Himalaya. *Geological Society of America Bulletin* **112**, 467–77.
- Ambrose TK, Larson KP, Guilmette C, Cottle JM, Buckingham H and Rai S (2015) Lateral Extrusion, underplating, and out-of-sequence thrusting within the Himalayan Metamorphic Core, Kanchenjunga, Nepal. *Lithosphere* **7**, 441–64.
- Antolín B, Appel E, Montomoli C, Dunkl I, Ding L, Gloaguen R and El Bay R (2011) Kinematic evolution of the eastern Tethyan Himalaya: constraints from magnetic fabric and structural properties of the Triassic flysch in SE Tibet. In: *Kinematic Evolution and Structural Styles of Fold-and-Thrust Belts* (eds J Poblet and R Lisle), **349**, pp. 99–121. Geological Society, Special Publications, London.
- Arita K (1983) Origin of the inverted metamorphism of the lower Himalayas, Central Nepal. *Tectonophysics* **95**, 43–60.
- Benetti B, Montomoli C, Iaccarino S, Langone A and Carosi R (2021) Mapping tectono-metamorphic discontinuities in orogenic belts: Implications for mid-crust exhumation in NW Himalaya. *Lithos* **392–393**, 106–29.
- Braden Z, Godin L and Cottle JM (2017) Segmentation and rejuvenation of the Greater Himalayan sequence in western Nepal revealed by in situ U–Th/Pb monazite petrochronology. *Lithos* **285**, 751–65.
- Braden Z, Godin L, Kellet DA and Yakymchuk C (2020) Spatio-temporal challenges in dating orogen-scale shear zones: the case of the Himalayan Main Central thrust. *Tectonophysics* **774**, 228–46.
- Bunge HJ (1982) *Texture Analysis in Materials Science, 1st Edition: Mathematical Methods*. London: Butterworth-Heinemann, 614 pp.
- Burchfiel BC, Chen Z, Hodges KV, Liu Y, Royden LH, Changrong D and Xu L (1992) The South Tibetan detachment system, Himalayan Orogen: extension contemporaneous with and parallel to shortening in a collisional mountain belt. *Geological Society of America Special Paper* **269**, 1–41.
- Burg JP, Brunel M, Gapais D, Chen GM and Liu GH (1984) Deformation of leucogranites of the crystalline Main Central Sheet in southern Tibet (China). *Journal of Structural Geology* **6**, 535–42.
- Burkhard M (1993) Calcite twins, their geometry, appearance and significance as stress-strain markers and indicators of tectonic regime: a review. *Journal of Structural Geology* **15**, 3–5, 351–68.
- Carosi R, Lombardo B, Molli G, Musumeci G and Pertusati PC (1998) The South Tibetan detachment system in the Rongbuk valley, Everest region. Deformation features and geological implications. *Journal of Asian Earth Sciences* **16**, 299–311.
- Carosi R, Montomoli C and Iaccarino S (2018) 20 years of geological mapping of the metamorphic core across Central and Eastern Himalayas. *Earth-Science Reviews* **177**, 124–38.
- Carosi R, Montomoli C, Iaccarino S, Benetti B, Petrocchia A and Simonetti M (2022) Constraining the timing of evolution of Shear zones in two collisional orogens: fusing structural geology and geochronology. *Geosciences* **12**, 231. doi: [10.3390/geosciences12060231](https://doi.org/10.3390/geosciences12060231).
- Carosi R, Montomoli C, Iaccarino S, Massonne H-J, Rubatto D, Langone A, Gemignani L and Visonà D (2016) Middle to late Eocene exhumation of the Greater Himalayan sequence in the Central Himalayas: progressive accretion from the Indian plate. *Geological Society of America Bulletin* **128**, 1571–92.
- Carosi R, Montomoli C, Iaccarino S and Visonà D (2019) Structural evolution, metamorphism and melting in the Greater Himalayan Sequence in Central-Western Nepal. *Geological Society London Special Publications* **483**, 305–23.
- Carosi R, Montomoli C, Rubatto D and Visonà D (2010) Late Oligocene high-temperature shear zones in the core of the Higher Himalayan Crystallines (Lower Dolpo, Western Nepal). *Tectonics* **29**, TC4029.
- Carosi R, Montomoli C, Rubatto D and Visonà D (2013) Leucogranite intruding the South Tibetan Detachment in western Nepal: implications for exhumation models in the Himalayas. *Terra Nova* **25**, 478–89. doi: [10.1111/ter.12062](https://doi.org/10.1111/ter.12062).
- Catlos EJ (2013) Generalizations about monazite: implications for geochronologic studies. *American Mineralogist* **98**, 819–32.
- Catlos EJ (2021) Records of Himalayan metamorphism and compressional tectonics in the central Himalayas (Darondi Khola, Nepal). In *Compressional Tectonics: Plate Convergence to Mountain Building* (eds I Cemen and EJ Catlos), Volume II, p. 2021. Washington, DC, USA: AGU Books; American Geophysical Union.
- Catlos EJ, Harrison TM, Kohn MJ, Grove M, Ryerson FJ, Manning CE and Upreti BN (2001) Geochronologic and thermobarometric constraints on the evolution of the Main Central Thrust, central Nepal Himalaya. *Journal of Geophysical Research-Solid Earth* **106**, 16177–204.
- Catlos EJ, Lovera OM, Kelly ED, Ashley KT, Harrison TM and Etzel T (2018) Modeling high-resolution pressure-temperature paths across the Himalayan Main Central Thrust (Central Nepal): Implications for the dynamics of collision. *Tectonics* **37**, 2363–88. doi: [10.1029/2018TC005144](https://doi.org/10.1029/2018TC005144).
- Catlos EJ, Perez TJ, Lovera OM, Dubey CS, Schmitt AK and Etzel TM (2020) High-resolution P-T-time paths across Himalayan faults exposed along the Bhagirathi transect NW India: implications for the construction of the Himalayan orogen and ongoing deformation. *Geochemistry, Geophysics, Geosystems* **21**, e2020GC009353.
- Chakraborty S, Mukul M, Mathew G and Pande K (2019) Major shear zone within the Greater Himalayan Sequence and sequential evolution of the metamorphic core in Sikkim, India. *Tectonophysics* **770**, 228183. doi: [10.1016/j.tecto.2019.228183](https://doi.org/10.1016/j.tecto.2019.228183).
- Colchen M, Le Fort P and Pêcher A (1986) *Annapurna-Manaslu-Ganesh Himal*. Paris: Centre National de la Recherches Scientifiques.
- Coleman ME (1996) Orogen-parallel and orogen-perpendicular extension in the central Nepalese Himalayas. *Geological Society of America Bulletin* **108**, 1594–607.



- Coleman ME** (1998) U-Pb constraints on Oligocene-Miocene deformation and anatexis within the central Himalaya, Marsyandi Valley, Nepal. *American Journal of Science* **298**, 553–71. doi: [10.2475/ajs.298.7.553](https://doi.org/10.2475/ajs.298.7.553).
- Coleman ME and Hodges VK** (1998) Contrasting Oligocene and Miocene thermal histories from the hanging wall and footwall of the South Tibetan detachment in the central Himalaya from  $^{40}\text{Ar}/^{39}\text{Ar}$  thermochronology, Marsyandi Valley, central Nepal. *Tectonics* **17**, 726–40.
- Corrie SL and Kohn MJ** (2011) Metamorphic history of the central Himalaya, Annapurna region, Nepal, and implications for tectonic models. *Geological Society of America Bulletin* **123**, 9–10, 1863–79.
- Cottle JM, Larson KP and Kellett DA** (2015) How does the mid-crust accommodate deformation in large, hot collisional orogens? A review of recent research in the Himalayan orogen. *Journal of Structural Geology* **78**, 119–33.
- Cottle J, Lederer G and Larson K** (2019) The monazite record of pluton assembly: mapping manaslu using petrochronology. *Chemical Geology* **530**, 119309. doi: [10.1016/j.chemgeo.2019.119309](https://doi.org/10.1016/j.chemgeo.2019.119309).
- Cottle JM, Kylander-Clark AR and Vrijmoed JC** (2012) U–Th/Pb geochronology of detrital zircon and monazite by single shot laser ablation inductively coupled plasma mass spectrometry (SS-LA-ICPMS). *Chemical Geology* **332**, 136–47.
- De Bresser JHP and Spiers CJ** (1997) Strength characteristics of the  $r$ ,  $f$ , and  $c$  slip systems in calcite. *Tectonophysics* **272**, 1–23.
- Di Vincenzo G, Carosi R and Palmeri R** (2004) The relationship between tectono-metamorphic evolution and argon isotope records in white mica: constraints from in situ  $^{40}\text{Ar}$ – $^{39}\text{Ar}$  Laser Analysis of the Variscan Basement of Sardinia. *Journal of Petrology* **45**, 1013–43.
- Dumond G, Mahan KH, Goncalves P, Williams ML and Jercinovic MJ** (2022) Monazite as a monitor of shear strain in orogenic crust. *Journal of Structural Geology* **161**, 104672.
- Dunkl I, Antolin B, Wemmer K, Rantitsch G, Kienast M, Montomoli C, Ding L, Carosi R, Appel E, El Bay R, Xu Q, von Eynatten H, Gloaguen R and Ratschbacher L** (2011) Metamorphic evolution of the Tethyan Himalayan flysch in SE Tibet. In: *Growth and Collapse of the Tibetan Plateau*, Geological Society, London, Special Publications **353**, pp. 45–69.
- Engi M** (2017) Petrochronology based on REE-minerals: monazite, allanite, xenotime, apatite. In: *Petrochronology: Methods and Applications* (M.J. Kohn, M. Engi, P. Lanari, eds). *Reviews in Mineralogy and Geochemistry* **83**, 365–418.
- Ferrill DA, Morris AP, Evans MA, Burkhard M, Groshong Jr RH and Onasch CM** (2004) Calcite twin morphology: a low-temperature deformation geothermometer. *Journal of Structural Geology* **26**, 1521–9.
- Frank W and Fuchs GR** (1970) Geological investigations in west Nepal and their significance for the geology of the Himalayas. *Geologische Rundschau* **59**, 552–80.
- Fossen H and Cavalcante GCG** (2017) Shear zones—a review. *Earth-Science Reviews* **171**, 434–55. doi: [10.1016/j.earscirev.2017.05.002](https://doi.org/10.1016/j.earscirev.2017.05.002).
- Gansser A** (1964) *Geology of the Himalayas*. New York: Interscience Publishers John Wiley and Sons, 289 pp.
- Garzanti E** (1999) Stratigraphy and sedimentary history of the Nepal Tethys Himalaya passive margin. *Journal of Asian Earth Science* **17**, 805–27.
- Gibson HD, Carr SD, Brown RL and Hamilton MA** (2004) Correlations between chemical and age domains in Monazite, and Metamorphic reactions involving major pelitic phases: an integration of ID-TIMS and SHRIMP geochronology with Y-Th-U X-ray mapping. *Chemical Geology* **211**, 237–60.
- Gibson R, Godin L, Kellett DA, Cottle J and Archibald D** (2016) Diachronous deformation along the base of the Himalayan metamorphic core, west-central Nepal. *Geological Society of America Bulletin* **128**, 860–78.
- Godin L, Grujic D, Law RD and Searle MP** (2006) Channel flow, ductile extrusion and exhumation in continental collision zones: an introduction. *Geological Society of London Special Publication* **268**, 1–23.
- Goscombe B, Gray D and Foster DA** (2018) Metamorphic response to collision in the Central Himalayan Orogen. *Gondwana Research* **57**, 191–265.
- Green OR, Searle MP, Corfield RI and Corfield RM** (2008) Cretaceous-Tertiary carbonate platform evolution and the age of the India-Asia collision along the Ladakh Himalaya (Northwest India). *Journal of Geology* **116**, 331–53.
- Guillot S, Hodges KV, Le Fort P and Pêcher A** (1994) New constraints of the age of the Manaslu leucogranite: evidence for episodic tectonic denudation in the central Himalayas. *Geology* **22**, 559–62.
- Guillot S, Le Fort P, Pêcher A, Barman MR and Aprahamian J** (1995) Contact metamorphism and depth of emplacement of the Manaslu granite (central Nepal). Implications for Himalayan orogenesis. *Tectonophysics* **241**, 99–119. doi: [10.1016/0040-1951\(94\)00144-X](https://doi.org/10.1016/0040-1951(94)00144-X).
- Handy MR** (1994) Flow laws for rocks containing two non-linear viscous phases: a phenomenological approach. *Journal of Structural Geology* **16**, 287–301.
- He D, Webb AAG, Larson KP, Martin AJ and Schmitt AK** (2015) Extrusion vs. duplexing models of Himalayan mountain building 3: duplexing dominates from the Oligocene to present. *International Geological Review* **57**, 1–27.
- Hébert R, Bezard R, Guilmette C, Dostal J, Wang CS and Liu ZF** (2012) The Indus–Yarlung Zangbo ophiolites from Nanga Parbat to Namche Barwa syntaxes, southern Tibet: first synthesis of petrology, geochemistry, and geochronology with incidences on geodynamic reconstructions of Neo-Tethys. *Gondwana Research* **22**, 377–97.
- Heim A and Gansser A** (1939) Central Himalaya: geological observations of the Swiss expedition 1936. *Mémoires de la Société helvétique des sciences naturelles* **73**, 1–245.
- Hielscher R and Schaeben H** (2008) A novel pole figure inversion method: specification of the MTEX algorithm. *Journal of Applied Crystallography* **41**, 1024–37. doi: [10.1107/S0021889808030112](https://doi.org/10.1107/S0021889808030112).
- Hodges KV** (2000) Tectonics of the Himalaya and southern Tibet from two perspectives. *Geological Society of America Bulletin* **112**, 324–50.
- Hu X, Garzanti E, Wang J, Huang W, An W and Webb A** (2016) The timing of India-Asia collision onset – facts, theories, controversies. *Earth-Science Reviews* **160**, 264–99.
- Hunter NJ, Weinberg RF, Wilson CJL, Luzin V and Misra S** (2019) Quartz deformation across interlayered monomineralic and polymineralic rocks: a comparative analysis. *Journal of Structural Geology* **119**, 118–34.
- Iaccarino S, Montomoli C, Carosi R, Massonne H-J, Langone A and Visonà D** (2015) Pressure–temperature–time–deformation path of kyanite-bearing migmatitic paragneiss in the Kali Gandaki valley (Central Nepal): investigation of Late Eocene-Early Oligocene melting processes. *Lithos* **231**, 103–21.
- Iaccarino S, Montomoli C, Carosi R, Massonne H-J and Visonà D** (2017a) Geology and tectono-metamorphic evolution of the Himalayan Metamorphic Core: insights from the Mugu Karnali transect, Western Nepal (Central Himalaya). *Journal of Metamorphic Geology* **35**, 301–25. doi: [10.1111/jmg.12233](https://doi.org/10.1111/jmg.12233).
- Iaccarino S, Montomoli C, Carosi R, Montemagni C, Massonne H-J, Langone A, Jain AK and Visonà D** (2017b) Pressure-temperature-deformation-time constraints on the South Tibetan Detachment System in the Garhwal Himalaya (NW India). *Tectonics* **36**, 2281–304.
- Iaccarino S, Montomoli C, Montemagni C, Massonne H-J, Langone A, Jain AK, Visonà D and Carosi R** (2020) The main central thrust zone along the Alaknanda and Dhauri Ganga valleys (Garhwal Himalaya, NW India): insights into an inverted metamorphic sequence. *Lithos* **372–373**, 105669. doi: [10.1016/j.lithos.2020.105669](https://doi.org/10.1016/j.lithos.2020.105669).
- Imayama T, Hoshino R, Keewok Y and Kawabata R** (2022) Eocene to Miocene metamorphic evolution and tectonic implication of the Ilam Nappe in Nepal Himalaya: constraints from P–T conditions and monazite petrochronology. *Journal of Asian Earth Sciences* **234**, 105276.
- Imayama T, Takeshita T, Yi K, Cho D-L, Kitajima K, Tsutsumi Y, Kayama M, Nishido H, Okumura T, Yagi K, Itaya T and Sano Y** (2012) Two-stage partial melting and contrasting cooling history within the Higher Himalayan Crystalline Sequence in the far-eastern Nepal Himalaya. *Lithos* **134–135**, 1–22.
- Kellett DA, Cottle JM and Larson KP** (2019) The South Tibetan detachment system: history, advances, definition and future directions. *Geological Society of London Special Publications* **483**, 377–400.
- Kellett DA, Grujic D, Warren C, Cottle J, Jamieson R and Tenzin T** (2010) Metamorphic history of a syn-convergent orogen-parallel detachment: the South Tibetan detachment system, Bhutan Himalaya. *Journal of Metamorphic Geology* **28**, 785–808.

- Khanal S, Robinson DM, Kohn MJ and Mandal S** (2015) Evidence for a far-traveled thrust sheet in the Greater Himalayan thrust system, and an alternative model to building the Himalaya. *Tectonics* **34**, 31–52.
- Kohn MJ** (2008) P-T-t data from Nepal support critical taper and repudiate large channel flow of the Greater Himalayan Sequence. *Geological Society of America Bulletin* **120**, 259–73.
- Kohn MJ** (2016) Metamorphic chronology, a tool for all ages: past achievements and future prospects. *American Mineralogist* **100**, 897–908.
- Kohn MJ, Engi M and Lanari P** (2017) Petrochronology: methods and applications. *Reviews in Mineralogy and Geochemistry* **83**, 582.
- Kohn MJ and Spear FS** (2000) Retrograde net transfer reaction insurance for pressure-temperature estimates. *Geology* **28**, 1127–30.
- Kohn MJ, Wieland MS, Parkinson CD and Upreti BN** (2005) Five Generations of Monazite in Langtang Gneisses: implications for chronology of the Himalayan metamorphic core. *Journal of Metamorphic Geology* **23**, 399–406.
- Kruhl JH** (1996) Prism- and basal-plane parallel subgrain boundaries in quartz: a microstructural geothermobarometer. *Journal of Metamorphic Geology* **14**, 581–9.
- Kylander-Clark ARC, Hacker BR and Cottle JM** (2013) Laser-Ablation split-stream ICP petrochronology. *Chemical Geology* **345**, 99–112.
- Larson K, Cottle J, Lederer G and Rai SM** (2017) Defining shear zone boundaries using fabric intensity gradients: an example from the east-central Nepal Himalaya. *Geosphere* **13**, 771–81.
- Larson KP, Ambrose TK, Webb AAG, Cottle MJ and Shrestha S** (2015) Reconciling Himalayan midcrustal discontinuities: the main central thrust system. *Earth and Planetary Science Letters* **429**, 139–46.
- Larson KP, Cottle JM and Godin L** (2011) Petrochronologic record of metamorphism and melting in the upper Greater Himalayan sequence, Manaslu–Himal Chuli Himalaya, west-central Nepal. *Lithosphere* **3**, 379–92. doi: [10.1130/L149.1](https://doi.org/10.1130/L149.1).
- Larson KP, Godin L and Price AR** (2010) Relationships between displacement and distortion in orogens: Linking the Himalayan foreland and hinterland in central Nepal. *Geological Society of American Bulletin* **122**, 1116–34.
- Law RD** (2014) Deformation thermometry based on quartz *c*-axis fabric and recrystallization microstructures: a review. *Journal of Structural Geology* **66**, 129–61.
- Law RD and Johnson MRW** (2010) Microstructures and crystal fabrics of the Moine thrust zone and Moine nappe: history of research and changing tectonic interpretations. In *Continental Tectonics and Mountain Building e The Legacy of Peach and Horne* (eds RD Law, RWH Butler, R Holdsworth, M Krabbendam and RA Strachan), 335, p. 443e503. Geological Society of London Special Publications, London.
- Law RD, Stahr DW, Francis MK, Ashley KT, Grasemann B and Ahmad T** (2013) Deformation temperatures and flow vorticities near the base of the Greater Himalayan Series, Sutlej Valley and Shimla Klippe, NW India. *Journal of Structural Geology* **54**, 21–53.
- Le Fort P** (1975) Himalaya: the collided range. *American Journal of Science* **275**, 1–44.
- Lister GS and Hobbs BE** (1980) The simulation of fabric development during plastic deformation and its application to quartzite: the influence of deformation history. *Journal of Structural Geology* **2**, 355–70.
- Long SP and Kohn MJ** (2020) Distributed ductile thinning during thrust emplacement: a commonly overlooked exhumation mechanism. *Geology* **8**, 368–73. doi: [10.1130/G47022.1](https://doi.org/10.1130/G47022.1).
- Martin AJ** (2017a) A review of definitions of the Himalayan Main Central Thrust. *International Journal of Earth Sciences* **106**, 2131–45.
- Martin AJ** (2017b) A review of Himalayan stratigraphy, magmatism, and structure. *Gondwana Research* **49**, 42–80.
- Martin AJ, Copeland P and Benowitz JA** (2015) Muscovite  $^{40}\text{Ar}/^{39}\text{Ar}$  ages help reveal the Neogene tectonic evolution of the southern Annapurna Range, central Nepal. *Geological Society of London Special Publications* **412**, 199–220.
- Martin AJ, Ganguly J and Decelles PG** (2010) Metamorphism of greater and lesser Himalayan rocks exposed in the Modi Khola valley, central Nepal. *Contributions to Mineralogy and Petrology* **159**, 203–23.
- Massonne H-J** (2012) Formation of amphibole and clinzoisite–epidote in eclogite owing to fluid infiltration during exhumation in a subduction channel. *Journal of Petrology* **53**, 1969–98.
- McKinney ST, Cottle JM and Lederer G** (2015) Evaluating rare earth element (REE) mineralization mechanisms in Proterozoic gneiss, Music Valley, California. *Geological Society of America Bulletin* **127**, 1153–2.
- Montemagni C, Carosi R, Fusi N, Iaccarino S, Montomoli C, Villa IM and Zanchetta S** (2020) Three-dimensional vorticity and time-constrained evolution of the Main Central Thrust zone, Garhwal Himalaya (NW India). *Terra Nova* **32**, 215–24. doi: [10.1111/ter.12450](https://doi.org/10.1111/ter.12450)
- Montomoli C, Carosi R and Iaccarino S** (2015) Tectonometamorphic discontinuities in the Greater Himalayan sequence: a local or a regional feature? In *Tectonics of the Himalaya* (eds S Mukherjee, R Carosi, PA van der Beek, BK Mukherjee and DM Robinson), 412, pp. 25–41, Geological Society, Special Publications, London.
- Montomoli C, Iaccarino S, Antolin B, Appel E, Carosi R, Dunkl I, Lin D and Visonà D** (2017) Tectono-metamorphic evolution of the Tethyan Sedimentary Sequence (Himalayas, SE Tibet). *Italian Journal of Geosciences* **136**, 73–88.
- Montomoli C, Iaccarino S, Carosi R, Langone A and Visonà D** (2013) Tectonometamorphic discontinuities within the Greater Himalayan Sequence in Western Nepal (Central Himalaya): insights on the exhumation of crystalline rocks. *Tectonophysics* **608**, 1349–70.
- Montemagni C, Iaccarino S, Montomoli C, Carosi R, Jain AK and Villa IM** (2018) Age constraints on the deformation style of the South Tibetan Detachment system in Garhwal Himalaya. *Italian Journal of Geosciences* **137**, 175–87. doi: [10.3301/IJG.2018.07](https://doi.org/10.3301/IJG.2018.07).
- Montemagni C, Montomoli C, Iaccarino S, Carosi R, Jain AK, Massonne HJ and Villa IM** (2019) Dating protracted fault activities: microstructures, microchemistry and geochronology of the Vaikrita Thrust, Main Central Thrust Zone, Garhwal Himalaya, NW India. *Geological Society of London Special Publication* **481**, 127–46.
- Mukhopadhyay DK, Chakraborty S, Trepmann C, Rubatto D, Anczkiewicz R, Gaidies F, Dasgupta S and Chowdhury P** (2017) The nature and evolution of the Main Central Thrust: Structural and geochronological constraints from the Sikkim Himalaya, NE India. *Lithos* **282–283**, 447–63. doi: [10.1016/j.lithos.2017.01.015](https://doi.org/10.1016/j.lithos.2017.01.015).
- Müller W, Aerden D and Halliday N** (2000) Isotopic dating of strain fringe increments: duration and rates of deformation in shear zones. *Science* **288**, 2195–8.
- Nania L** (2021) Unravelling the evolution of regional-scale shear zones with the aid of microstructures and textural analysis: an example from the central Himalaya. *Rendiconti Online Della Società Geologica Italiana* **54**, 32–40. doi: [10.3301/ROL.2021.07](https://doi.org/10.3301/ROL.2021.07).
- Nania L, Montomoli C, Iaccarino S, Leiss B and Carosi R** (2022) Multi-stage evolution of the South Tibetan Detachment system in central Himalaya: Insights from carbonate-bearing rocks. *Journal of Structural Geology* **158**, 104574. doi: [10.1016/j.jsg.2022.104574](https://doi.org/10.1016/j.jsg.2022.104574).
- Parrish RR and Hodges KV** (1996) Isotopic constraints on the age and provenance of the lesser and greater Himalayan sequences, Nepalese Himalaya. *Geological Society American Bulletin* **108**, 904–11.
- Parsons AJ, Ferré EC, Law RD, Lloyd GE, Phillips RJ and Searle MP** (2016a) Orogen-parallel deformation of the Himalayan midcrust: insights from structural and magnetic fabric analyses of the Greater Himalayan sequence, Annapurna–Dhaulagiri Himalaya, central Nepal. *Tectonics* **35**, 2515–37.
- Parsons AJ, Law RD, Lloyd GE, Phillips RJ and Searle MP** (2016b) Thermo-kinematic evolution of the Annapurna–Dhaulagiri Himalaya, Central Nepal: the composite Orogenic system. *Geochemistry, Geophysics, Geosystems* **17**, 1511–39.
- Parsons AJ, Law RD, Searle MP, Phillips RJ and Lloyd GE** (2016c) Geology of the Dhaulagiri–Annapurna–Manaslu Himalaya, Western region, Nepal, 1:200,000. *Journal of Maps* **12**, 100–10.
- Passchier CW and Trouw RAJ** (2005) *Microtectonics*. Berlin Heidelberg: Springer, p. 366 .
- Pêcher A** (1989) The metamorphism in the Central Himalaya. *Journal of Metamorphic Geology* **7**, 31–41.

- Pêcher A** (1991) The contact between the Higher Himalaya Crystallines and the Tibetan sedimentary series: miocene large-scale dextral shearing. *Tectonics* **10**, 587–98.
- Pêcher A and Fort M** (2012) Géologie autour du Manaslu (un trek au Népal central), 1–56. <https://www.isterre.fr/IMG/pdf/manaslu-livret-2013.pdf>.
- Pêcher A and Le Fort P** (1986) The metamorphism in central Himalaya, its relations with thrust tectonics. In *Evolution des domaines orogéniques d'Asie méridionale (de la Turquie à l'Indonésie)* (eds P Le Fort, M Cholchen and C Montenat), pp. 285–309. Paris: Science de la Terre.
- Powell R and Holland T** (1994) Optimal geothermometry and geobarometry. *American Mineralogist* **79**, 120–33.
- Powell R and Holland TJB** (2008) On thermobarometry. *Journal of Metamorphic Geology* **26**, 155–79.
- Pyle JM** (2006) Temperature-time paths from phosphate accessory phase paragenesis in the Honey Brook Upland and associated cover sequence, SE Pennsylvania, USA. *Lithos* **88**, 201–32.
- Pyle JM and Spear FS** (1999) Yttrium zoning in garnet: coupling of major and accessory phases during metamorphic reactions. *Geological Materials Research* **1**, 1–49.
- Pyle JM and Spear FS** (2003) Four generations of accessory-phase growth in low-pressure migmatites from SW New Hampshire. *American Mineralogist* **88**, 338–51.
- Pyle JM, Spear FS, Wark DA, Daniel CG and Storm LC** (2005) Contributions to precision and accuracy of monazite microprobe ages. *American Mineralogist* **90**, 547–77.
- Roberts AG, Weinberg RF, Hunter NJR and Ganade CE** (2020) Large-scale rotational motion within the main central thrust zone in the Darjeeling-Sikkim Himalaya, India. *Tectonics* **39**, 12. doi: [10.1029/2019TC005949](https://doi.org/10.1029/2019TC005949).
- Rubatto D, Chakraborty S and Dasgupta S** (2013) Timescales of crustal melting in the higher Himalayan Crystallines (Sikkim, Eastern Himalaya) inferred from trace element-constrained monazite and zircon chronology. *Contributions to Mineralogy and Petrology* **165**, 349–72.
- Rubatto D, Schaltegger U, Lombardo B, Colombo F and Compagnoni R** (2001) Complex Paleozoic magmatic and metamorphic evolution in the Argentera Massif (Western Alps) resolved with U–Pb dating. *Schweizerische Mineralogische und Petrographische Mitteilungen* **81**, 213–28.
- Schaeben H** (1997) A simple standard orientation density function: the hyperspherical de la Vall'ée Poussin kernel. *Physica status solidi (b)* **200**, 367–76.
- Schneider C and Marsh L** (1993) The metamorphism of the Tibetan series from the Manang area, Marsyandi valley, central Nepal. *Geological Society of London Special Publications* **74**, 357–74.
- Schulz B** (2021) Monazite microstructure and their interpretation in petrochronology. *Frontiers in Earth Science* **9**, 668566.
- Searle MP** (2010) Low-angle normal faults in the compressional Himalayan orogen: evidence from the Annapurna-Dhaulagiri Himalaya, Nepal. *Geosphere* **6**, 296–315.
- Searle MP** (2013) Crustal melting, ductile flow and deformation in mountain belts: cause and effect relationships. *Lithosphere* **5**, 547–54.
- Searle MP** (2019) Timing of subduction initiation, arc formation, ophiolite obduction and India-Asia collision in the Himalaya. In *Himalaya Tectonics a Modern Synthesis* (eds PJ Treloar and MP Searle), **483**, pp. 19–38. Geological Society, Special Publication, London.
- Searle MP and Godin L** (2003) The South Tibetan Detachment System and the Manaslu Leucogranite: a structural reinterpretation and restoration of the Annapurna–Manaslu Himalaya, Nepal. *Journal of Geology* **111**, 505–23.
- Searle MP, Law RD, Godin L, Larson K, Streule MJ, Cottle JM and Jessup MJ** (2008) Defining the Himalayan Main Central Thrust in Nepal. *Journal of the Geological Society* **165**, 523–34.
- Searle MP, Simpson RL, Law RD, Parrish RR and Waters DJ** (2003) The structural geometry, metamorphic and magmatic evolution of the Everest massif, High Himalaya of Nepal–South Tibet. *Journal of the Geological Society* **160**, 345–66.
- Shrestha S, Larson KP, Martin AJ, Guilmette C, Smit MJ and Cottle JM** (2020) The greater Himalayan thrust belt: insight into the assembly of the exhumed Himalayan Metamorphic Core, Modi Khola Valley, Central Nepal. *Tectonics* **39**, e2020TC006252. doi: [10.1029/2020TC006252](https://doi.org/10.1029/2020TC006252).
- Skemer P, Katayama I, Jiang Z and Karato SI** (2005) The misorientation index: development of a new method for calculating the strength of lattice-preferred orientation. *Tectonophysics* **411**, 157–67.
- Soucy La Roche R, Dyer SC, Zagorevski A, Cottle JM and Gaidies F** (2022) 150 Myr of episodic metamorphism recorded in the Yukon-Tanana Terrane, Northern Canadian Cordillera: evidence from monazite and xenotime petrochronology. *Lithosphere* **1**, 7708357. doi: [10.2113/2022/7708357](https://doi.org/10.2113/2022/7708357).
- Soucy La Roche R and Godin L** (2019) Inherited cross-strike faults and oligocene-early miocene segmentation of the main Himalayan Thrust, West Nepal. *Journal of Geophysical Research: Solid Earth* **124**, 619–7518.
- Soucy La Roche R, Godin L, Cottle JM and Kellett DA** (2018) Preservation of the early evolution of the Himalayan middle crust in foreland klippen: insights from the Karnali klippe, west Nepal. *Tectonics* **37**, 1161–93.
- Spear FS, Kohn MJ and Cheney JT** (1999) P – T paths from anatectic pelites. *Contributions to Mineralogy and Petrology* **134**, 17–32. doi: [10.1007/s004100050466](https://doi.org/10.1007/s004100050466).
- Spear FS and Menard T** (1989) Program GIBBS; a generalized Gibbs method algorithm. *American Mineralogist* **74**, 942–3.
- Spear FS and Pyle JM** (2010) Theoretical modeling of monazite growth in a low-Ca metapelite. *Chemical Geology* **273**, 111–9.
- Stipp M, Stunitz H, Heilbronner R and Schmid SM** (2002) The eastern Tonale fault zone: a “natural laboratory” for crystal plastic deformation of quartz over a temperature range from 250 to 700°C. *Journal of Structural Geology* **24**, 1864–84.
- Tomkins HS, Powell R and Ellis DJ** (2007) The pressure dependence of the zirconium-in-rutile thermometer. *Journal of Metamorphic Geology* **25**, 703–13. doi: [10.1111/j.1525-1314.2007.00724.x](https://doi.org/10.1111/j.1525-1314.2007.00724.x).
- Upreti BN and Le Fort P** (1999) Lesser Himalayan crystalline nappes of Nepal: problems of their origin. In *Himalaya and Tibet: Mountain Roots to Mountain Tops*: Geological Society of America. doi: [10.1130/0-8137-2328-0.225](https://doi.org/10.1130/0-8137-2328-0.225).
- Valdiya KS, Paul SK, Tarachandra-Bhakuni SS and Upadhyay RC** (1999) Tectonic and lithological characterization of Himadri (Great Himalaya) between Kali and Yamuna rivers, Central Himalaya. *Himalayan Geology* **10**, 1–17.
- Vannay J-C and Hodges KV** (1996) Tectonometamorphic evolution of the Himalayan metamorphic core between the Annapurna and Dhaulagiri, central Nepal. *Journal of Metamorphic Geology* **14**, 635–56.
- Villa IM** (2016) Diffusion in mineral geochronometers: present and absent. *Chemical Geology* **420**, 1–10. doi: [10.1016/j.chemgeo.2015.11.001](https://doi.org/10.1016/j.chemgeo.2015.11.001).
- Villa IM, Hermann J, Muntener O and Trommsdorff V** (2000) <sup>39</sup>Ar-<sup>40</sup>Ar dating of multiply zoned amphibole generations (Malenco, Italian Alps). *Contributions to Mineralogy and Petrology* **140**, 363–81.
- Visonà D, Carosi R, Montomoli C, Peruzzo L and Tiepolo M** (2012) Miocene andalusite leucogranite in central-east Himalaya (Everest–Masang Kang area): low-pressure melting during heating. *Lithos* **144**, 194–208.
- Wallis S** (1992) Vorticity analysis in a metachert from the Sanbagawa belt, SW Japan. *Journal of Structural Geology* **14**, 271–80.
- Walters JB and Kohn MJ** (2017) Protracted thrusting followed by late rapid cooling of the Greater Himalayan Sequence, Annapurna Himalaya, Central Nepal: Insights from titanite petrochronology. *Journal of Metamorphic Geology* **35**, 897–917. doi: [10.1111/jmg.12260](https://doi.org/10.1111/jmg.12260).
- Wang JM, Rubatto D and Zhang JJ** (2015) Timing of partial melting and cooling across the Greater Himalayan Crystalline complex (Nyalam, central Himalaya): in-sequence thrusting and its implications. *Journal of Petrology* **56**, 1677–702.
- Wang JM, Zhang JJ, Liu K, Zhang B, Wang XX, Rai SM and Scheltens M** (2016) Spatial and temporal evolution of Tectonometamorphic discontinuities in the central Himalaya: constraints from P-T paths and geochronology. *Tectonophysics* **679**, 41–60.
- Waters DJ** (2019) Metamorphic constraints on the tectonic evolution of the High Himalaya in Nepal: the art of possible. In *Himalaya Tectonics a Modern Synthesis* (eds PJ Treloar and MP Searle), **483**, pp. 325–75. Geological Society, Special Publication, London.
- Webb AAG, Yin A, Harrison TM, Célérier J and Burgess WP** (2007) The leading edge of the Greater Himalayan Crystalline complex revealed in the

- NW Indian Himalaya: implications for the evolution of the Himalayan orogen. *Geology* **35**, 955–8.
- Weinberg RF** (2016) Himalayan leucogranites and migmatites: nature, timing and duration of anatexis. *Journal of Metamorphic Geology* **34**, 821–43.
- Wenk HR, Takeshita T, Bechler E, Erskine BG and Matthies S** (1987) Pure shear and simple shear calcite textures. Comparison of experimental, theoretical and natural data. *Journal of Structural Geology* **9**, 731–45.
- Williams ML and Jercinovic MJ** (2002) Microprobe monazite geochronology: putting absolute time into microstructural analysis. *Journal of Structural Geology* **24**, 1013–28.
- Williams ML and Jercinovic MJ** (2012) Tectonic interpretation of metamorphic tectonites: integrating compositional mapping, microstructural analysis and in situ monazite dating. *Journal of Metamorphic Geology* **30**, 739–52.
- Williams ML, Jercinovic MJ and Hetherington CJ** (2007) Microprobe monazite geochronology: understanding geologic processes by integrating composition and chronology. *Annual Review of Earth and Planetary Sciences* **35**, 137–75.
- Williams ML, Jercinovic MJ and Terry M** (1999) High resolution “age” mapping, chemical analysis, and chemical dating of monazite using the electron microprobe: a new tool for tectonic analysis. *Geology* **27**, 1023–26.
- Yakymchuk C and Godin L** (2012) Coupled role of deformation and metamorphism in the construction of inverted metamorphic sequences: an example from far-northwest Nepal. *Journal of Metamorphic Geology* **30**, 513–35.
- Zeiger K, Gordon SM, Long SP, Kylander-Clark ARC, Agustsson K, Penfold M** (2015) Timing and conditions of metamorphism and melt crystallization in Greater Himalayan rocks, eastern and central Bhutan: insight from U–Pb zircon and monazite geochronology and trace-element analyses. *Contributions to Mineralogy and Petrology* **169**, article number: 47.